Evolution of fluid chemistry and fluid flow pathways during fold growth: an example from Taemas, NSW, Australia

Shaun L.L. Barker[1,*] · Stephen F. Cox[1]

[1]Research School of Earth Sciences, The Australian National University, Canberra, ACT 0200, Australia

[*]Current address: Department of Earth and Ocean Sciences, University of British Columbia, Vancouver, BC V6T1Z4, Canada

Abstract

In the Taemas area, New South Wales, Australia, a swarm of hydrothermal calcite and quartz veins are hosted in upright, open to close folded limestones and shales. Overprinting relationships and vein geometries demonstrate that the vein swarm formed during fold growth and associated reverse faulting. Textures preserved in veins reveal that veins formed via hundreds to thousands of individual dilation and mineral precipitation events. Bedding-parallel flexural slip during fold growth was associated with vein development, and limb-parallel stretching during fold growth was associated with the formation of bedding-orthogonal extension veins. The presence of subhorizontal extension fractures and severly misoriented faults imply that fluid pressures exceeded lithostatic levels, at least transiently, during the development of the vein swarm.

Vein $\delta^{18}O$ compositions systematically increase upwards through the Murrumbidgee Group, in response to progressive reaction of an externally derived, upwards flowing low-$\delta^{18}O$ fluid (of probable meteoric origin) with host limestones. Vein $\delta^{18}O$ and $^{87}Sr/^{86}Sr$ compositions vary spatially and temporally within the same outcrop, and within individual veins. These variations are inferred to be

caused by the ascent of packages of fluid along constantly changing flow pathways, caused by multiple permeability creation-destruction cycles associated with seismic rupture and fault sealing. Vein trace and rare earth element concentrations are more variable, likely reflecting rapid (< 10 m) rock buffering along fluid pathways.

Overpressured fluids allowed bedding-parallel slip to continue throughout fold growth, inhibiting the formation of crosscutting faults, and limiting the number of larger faults that formed. The generation of a backbone flow network would release high-pressure fluids, causing flexural slip to halt. This had not occurred by the time crustal shortening ceased in the Taemas area.

Introduction

Syntectonic veins record information on spatial and temporal variations of fluids migrating through the crust during progressive deformation and associated vein growth *(e.g.* Dietrich et al, 1983; Rye and Bradbury, 1988). Exhumed vein systems contain a record of where fluid flow was localised, how flow has influenced the mechanical behaviour of the crust, and the nature of chemical reactions between rocks and fluids along fluid flow pathways. Vein chemistry may also provide constraints on the nature of fluid reservoirs contributing to fluid flow during crustal deformation.

As externally-sourced fluids react with rocks, they become progressively rock-buffered along fluid flow pathways (Fig. 1). Many studies have been carried out exploring how fluid flow and fluid-rock reaction processes may affect the chemical and isotopic composition of host rocks and hydrothermal veins *(e.g.* Bickle and McKenzie, 1987; Lassey and Blattner, 1988; Rye and Bradbury, 1988; Bowman et al, 1994; Gerdes et al, 1995; McCaig et al, 1995; DePaolo and Getty, 1996; Abart and Sperb, 1997; Eppel and Abart, 1997; Steefel and Lichtner, 1998; Abart and Pozzorini, 2000; McCaig et al, 2000; Knoop et al, 2002; Badertscher et al, 2002;

Matthaei, 2003; Steefel et al, 2005; DePaolo, 2006; Cox, 2007; Zack and John, 2007). Many of these studies have assumed "steady state" fluid flow, without considering the influence that dynamic changes in permeability, with both time and space, will have on resulting fluid and vein compositions.

An extensive fold and fault-related vein network (hereafter called the 'Taemas Vein Swarm', or TVS) composed mainly of calcite veins, is developed throughout much of an interbedded limestone and shale sequence (the Murrumbidgee Group) in the Taemas area. The vein swarm is localized mainly within an area of approximately 20 km^2. Vein development and folding were synchronous, with a variety of bedding-discordant fault veins, bedding-parallel fault veins and extension veins developed. Laminated veins related to bedding-parallel slip are common, particularly in thinly interbedded limestone-mudstone units. Bedding-discordant faults, fault-related extension veins, and extension veins related to flexural flow and bedding-parallel stretching of fold limbs are also found.

The aim of this paper is to use spatial and temporal variations in vein isotopic and trace element composition in order to explore the dynamics of fluid flow and fluid-rock reaction in a fracture-

controlled hydrothermal system which was active during progressive crustal shortening.

Geological Setting of the Taemas Vein Swarm

The Taemas area is located southwest of Yass, in the Eastern Belt of the Lachlan Orogen, in eastern New South Wales, Australia (Glen, 1992). Here, a major fold triplet (Wee Jasper Syncline, Narrangullen Anticline, Taemas Synclinorium) form the larger Black Range Synclinorium (approximately 180 km long, 25 km wide). The Taemas Synclinorium is a doubly-plunging synclinorial structure approximately 5 km wide (Cramsie et al, 1975; Fig. 2). Within the Taemas Synclinorium, sedimentary rocks of the Murrumbidgee Group (Table 1) have been folded into upright, open to close folds (wavelengths varying between tens-of-metres to kilometre scale), which have a predominant north-northwest trend, and steep axial surfaces (Fig. 3). The synclinorium is to the west of the major, steeply-dipping, Warroo and Deakin - Devil's Pass Fault system. Here, Silurian volcanics overthrust the Murrumbidgee Group sediments (Cramsie et al, 1975). Within the Taemas Synclinorium, the Murrumbidgee Group is approximately 1 km thick, and is

composed of several limestone and shale formations, which were deposited during the middle Devonian (Browne, 1958; see Table 1 for stratigraphy and formation name abbreviations).

At the base of the sedimentary sequence (in the Sugarloaf Creek, SLC, formation and the underlying volcanic basement) bedding dips are low (typically < 20°) and bedding is gently folded, with fold wavelengths in the order of hundreds of metres to more than 1 km. Higher in the sequence, particularly in the Cavan Bluff Limestone (CBL), Spirifer yassensis Limestone (SYL) and Blomfield Limestone (BFL), close to tight folds occur, with shorter fold wavelengths (tens-to-hundreds of metres; see Figs. 3, 4). The shorter fold wavelength in the interbedded limestone-shale units (SYL and BFL) compared with the thicker, more competent underlying and overlying units (Majurgong Formation (MJF) and Receptaculites Limestone, RCL) indicates that localized mechanical decoupling occurred along bedding, reflecting a control of bed thickness on fold wavelength.

Cleavage is strongly developed in the MJF, and shaley beds in the SYL and BFL. Within sandstone beds in the MJF, cleavage fans strongly around outcrop-scale folds, typically at high angle to

bedding. This implies that layer-parallel shortening occurred early during fold growth, with subsequent buckling of bedding. In general, shales beds have a penetrative slaty cleavage, while limestone beds are internally unstrained, or contain a weak pressure-solution cleavage. Total strain, calculated by dividing bed lengths over a particular distance in cross section, is in the range of 20–50 %. Given geological strain rates in the order of 10^{-14} s^{-1} to 10^{-15} s^{-1} (Pfiffner and Ramsay, 1982; Mueller et al, 2000), this would imply that folding occurred over a period of 0.5 Ma to 15 Ma.

The Taemas Vein Swarm

Veins occur as:

1. Fault veins - veins which cut across, and displace bedding along shear fractures.
2. Bedding-parallel veins - veins which are concordant to bedding and have evidence for shear such as laminations and slickenfibres.
3. Extension veins - veins which have no evidence for shear displacement.

Shear veins

Shear veins, present as both bedding-discordant and bedding-parallel structures are found throughout the Taemas Vein Swarm. Fault veins crosscut and displace bedding, and are found in several outcrops. Fault veins are dominantly calcite, with minor quartz and rare fluorite. Extension veins are common around bedding-discordant faults. In addition, sub-vertical, apparently late, strike-slip faults cut bedding.

Displaced marker beds and the size of dilational jogs indicates that the majority of fault veins have net slip in the order of centimetres. However, at least three mapped faults have displacements up to metres to a few tens-of-metres, based on stratigraphic relationships.

Commonly, bedding-parallel and bedding-discordant veins are connected. One of the most spectacular sites of calcite veining in the TVS occurs where a bedding-parallel fault becomes bedding discordant, and displaces two anticlines against one another generating a dilatant site (Fig. 2, locality 2; Fig 5), which would have been a zone of high paleopermeability (*cf.* Cox, 2005).

Bedding-parallel veins

Bedding-parallel veins commonly contain tens to hundreds of mesoscopic grey-brown laminations, which lie subparallel to the

vein margins. Laminations are usually striated, and generally subperpendicular to the strike of the BPV, particularly on veins dipping at more than 40°. However while the trend of striations on several low-angle bedding-parallel veins at Shark's Mouth Peninsula (Fig 2, locality 4) varied over 55° on different laminae in the same vein. The dip of BPV varies between 20° and ~ 80°. Most veins have dips of 40° to 60°.

The laminated, bedding-parallel veins are analagous to those described by Gaviglio (1986); Tanner (1989); Jessell et al (1994) and Fowler (1996, and references therein). Slickenfibres and slickenlines found on laminations in the bedding-parallel veins record the slip vector. The gentle dip of some BPV (c. 20°) with highly variable striae orientation suggests that flexural slip begins at an early stage of folding, with variable slip vectors. As folds begin to tighten, and fold hinges become well defined, slip vectors become more consistent.

Some BPV may be traced directly around folds. The presence of BPV in fold hinge zones, and asymmetrically folded laminations within BPV suggest that ongoing fold growth postdated initial flexural slip. It seems likely that during the initial stages of folding,

significant strain is accommodated via slip between bedding layers. However, as bedding dips increase during folding, frictional lockup will occur (Ramsay, 1974). At this point slip on BPV may cease, and new faults may form which cut across bedding. Saddle reefs indicate that dilation occurs at some fold hinges during fold amplification.

Extension veins

Fold limbs rotated into steep orientations have undergone limb-parallel stretching, resulting in incipient bedding boudinage and associated subhorizontal extension veins (Fig. 6). Extension veining of this type is most prevalent in the CJL. This is likely due to the high competence of the CJL relative to the surrounding interbedded limestone-shale of the SYL and BFL.

On the east side of Taemas Peninsula (Locality 3, Fig. 2), calcite extension veins cut cleavage at a high angle on the limbs of both anticlines. A bedding-parallel vein is present between the two anticlines is cut by extension veins, which dip east (342/37E). The bedding-parallel vein is interpreted to be the result of flexural slip during folding. The high angle of calcite extension veins to cleavage within folds is consistent with veins formed during flexural flow

folding (Ramsay and Huber, 1987). Extension veins crosscutting the bedding-parallel vein imply that strain may be accommodated via flexural flow folding after bedding-parallel slip ceases, due to frictional lock up of beds (Ramsay, 1974). It is noted that *en echelon* arrays of flexural flow related veins form only in semi-competent and incompetent beds, and do not form within more competent massive limestone beds.

Extension veins show mutually overprinting relationship with cleavage (in shale rich beds) and stylolites (in more massive limestones). This implies that extension vein formation and folding were contemporaneous. Extension veins sometimes show mutually overprinting relationships to one another (Figs. 6c,e), implying that the orientation of σ_3 (at least locally) has changed dynamically over time.

In summary, various vein types formed throughout crustal shortening, and the growth history of different veins may be inferred. Thus, vein chemistry may be used to track variations in fluid composition ($\delta^{18}O$, $^{87}Sr/^{86}Sr$, trace and rare earth elements), which reflects changes in fluid source and the degree of fluid-rock

interaction, in both time and space.

Vein Textures

Veins dominantly have massive, laminated and fibrous textures, with elongate-blocky and crustiform textures also occurring. Bedding-parallel and fault veins have massive and laminated textures, with fibrous textures preserved in some parts of fault and bedding-parallel veins. Conversely, extension veins have massive, elongate-blocky or fibrous textures (laminated textures are absent in extension veins). It is emphasised here the particular textures are not isolated to specific host lithologies, and different textures are found both within the same outcrop, and within the same vein. Notably, veins may contain both fibrous and massive calcite, and massive and fibrous extension veins show mutually overprinting relations.

Laminated textures in bedding-parallel slip veins have been classified according to the terminology of Koehn and Passchier (2000). *Inclusion bands* are thin, dark bands parallel to the vein margins. *Crack-seal bands* are thin, dark bands between parallel inclusion bands, at angles of 20 to 35º to inclusion bands (Fig. 7). Crack-seal bands are typically separated by distances of 100 μm to 2

mm in laminated veins, and hundreds of crack-seal bands may occur in an interval of around 10 cm along one calcite lamina. Crack-seal bands are inferred to have formed along dilational sites during slip along laminations on the BPV (Koehn and Passchier, 2000).. It is suggested that each crack-seal band formed during one episode of slip, possibly during individual microseismic slip events

Geochemical Methods

Sample collection

The position and structural relationships of veins were recorded in the field prior to sample collection (see Appendix for sampling locations and complete analytical results). Unaltered host rock (at distances of more than 50 m from any visible veins) was collected from the Cavan Bluff, Spirifer yassensis, Currajong, Bloomfield and Receptaculites Limestones.

Stable isotope analysis

Oxygen and carbon isotope ratios for carbonates were measured on a

Finnigan MAT251 mass spectrometer. For each sample, 200 ± 20 μg of carbonate powder was dissolved in 103% H_3PO_4 at 90° in an automated carbonate (Kiel) device. Carbon isotope ratios are reported relative to Vienna Peedee Belemnite (VPDB). Oxygen isotope results are reported relative to VSMOW, and were converted from VPDB values, where:

$$\delta^{18}O_{VSMOW}=1.03091*\delta^{18}O_{VPDB}+30.91$$

(Coplen et al., 1983).

Isotope results have been normalised on the VSMOW and VPDB scales so that analyses of:

NBS-19 $\delta^{18}O_{VPDB}$= -2.20 ‰; $\delta^{18}O_{SMOW}$ = + 28.64 ‰ and $\delta^{13}C_{VPDB}$ = +1.95 ‰

NBS-18 $\delta^{18}O_{VPDB}$ = -23.0 ‰; $\delta^{18}O_{SMOW}$ = + 7.2 ‰ and $\delta^{13}C_{VPDB}$ = -5.0 ‰

The standard deviation (2 σ) for the 50 replicate NBS-19 standards used during the analysis of these samples was 0.02 ‰ for $\delta^{13}C$ and 0.06 ‰ for $\delta^{18}O$.

Quartz oxygen isotope ratios were measured at the University of

New Mexico. Quartz samples were separated from calcite (the calcite was stored for oxygen isotope analysis, as outlined above), and the quartz chips were placed into a 1M HCl solution, until all effervescence had ceased and calcite was removed.

The resulting quartz separates were examined using a binocular microscope, and clear quartz pieces were selected for analysis by laser fluorination (following the method of Sharp, 1990). An internal laboratory standard (Lausanne-1) was analysed to determine the reproducibility of analyses (±0.2 ‰).

Strontium isotope analyses

Host rock

Sr isotope compositions of host rock carbonate were measured by thermal ionising mass spectrometry (TIMS). Approximately 1 kg of each of two samples from each limestone member (10 samples total) was crushed using a tungsten carbide swing mill. Around 0.06 to 0.11 g of rock powder was placed into a clean Teflon® screw-cap vial. To separate only the carbonate component of the limestones, 1 mL of distilled 1 M acetic acid was added to each beaker, resulting in immediate, gentle effervescence. The beakers were allowed to rest

for 2 hours at room temperature, and 1 further mL of acetic acid was added, after which effervescence ceased. The resulting mixture of solution and sediment was centrifuged in clean tubes, and the liquid was drawn off and dried on hot plates. The samples were then taken up in HNO_3 for loading onto cation-exchange columns, where Sr was separated from other matrix elements. Rubidium was not collected or analysed, as Rb concentrations in carbonate are generally very low (Faure and Powell, 1972), and were confirmed to be very low (<1 ppm) by LA-ICPMS analyses (see below).

Purified Sr was loaded in H_3PO_4 on Ta filaments and analysed on a Finnigan Mat261 mass spectrometer. All filaments were outgassed for 30 minutes prior to loading. Sr isotope values were normalised to $^{86}Sr/^{88}Sr = 0.1194$. The NIST SRM-987 Sr isotope standard analysed had a $^{87}Sr/^{86}Sr$ value of 0.71023 ± 0.00001.

Carbonate veins

Sr isotope compositions were analysed on the same samples on which trace element analyses were conducted. Analyses were made using *in situ* laser ablation multi-collector inductively coupled plasma mass spectrometry (LA-MC-ICP-MS), and results of vein analyses are reported in the appendix. Analyses were carried out

using a HelEx ArF excimer laser ablation system, interfaced to a Finnigan MAT Neptune MC-ICP-MS (see Eggins et al, 1998, 2005, for details). Analyses were performed using a single spot approach (with a laser spot diameter of 137-233 μm). Laser pulse rates of 5 Hz in combination with a laser fluence of 5 J/cm, short laser wavelength (λ= 193 nm), and aperture imaging optics were used to attain controlled calcite ablation (~1 μm per second) in a He ablation medium (Eggins et al, 1998).

The moveable array of 9 Faraday cups were located to monitor all Sr isotopes and peak-strip key interfering species (Kr, Rb and REE). Faraday cups were positioned to the high mass-side of peak-centres to minimize potential REE overlaps following the approach of Ramos et al (2004). The gas flow and electrostatic lens settings were optimized for maximum Sr sensitivity and peak-shape while ablating a modern *Tridachna* clam shell which has a measured $^{87}Sr/^{86}Sr$ value of 0.709143±15 (Woodhead et al, 2005).

Tridachna was additionally used to monitor instrument reproducibility and accuracy. For 22 analyses of *Tridachna,* the average $^{87}Sr/^{86}Sr$ ratio was 0.709149±38 *(2 σ)*. Further details of analytical procedures are given in Barker et al. (2006).

Trace element analyses

Host rock

The trace element compositions of the carbonate component of limestone host rocks were measured by solution ICP-MS. A known amount of approximately 50–60 mg of rock powder was placed into a clean Teflon® screw-cap vial. To separate only the carbonate component of the limestones, 1 mL of distilled 1 M acetic acid was added to each beaker resulting in immediate, gentle effervescence. The beakers were allowed to rest for 2 hours at room temperature, and 1 further mL of acetic acid was added, after which effervescence ceased. The resulting mixture of solution and sediment was centrifuged in clean tubes, and the liquid was drawn off, dried on hot plates and taken up in around 100 mL of 2% HNO_3 for analysis. Trace elements were measured using a quadrupole ICP-MS (Agilent 7500s) running in solution mode. Multiple major and trace elements (^{9}Be, ^{23}Na,^{25}Mg, ^{29}Si, ^{31}P, ^{45}Sc, ^{49}Mn, ^{57}Fe, ^{75}As, ^{85}Rb, ^{86}Sr, ^{89}Y, ^{115}In, ^{137}Ba, ^{139}La, ^{140}Ce, ^{141}Pr, ^{146}Nd, ^{147}Sm, ^{151}Eu, ^{158}Gd, ^{163}Dy, ^{165}Er, ^{166}Er, ^{174}Yb, ^{175}Lu, ^{185}Re, ^{208}Pb, ^{209}Bi, ^{232}Th, ^{238}U) were analysed, with multiple internal standards (Be, As, In, Re, Bi) to monitor instrument performance and drift.

Carbonate veins

Veins were analysed for trace element compositions using a multiple spot analysis, laser ablation ICP-MS approach. Samples were analysed using a pulsed ArF Excimer laser (λ=193 nm) and a quadrupole ICP-MS (Agilent 7500s Eggins et al, 1998). Samples were precleaned with ethanol. Every vein sample was analysed between 3 to 10 times using a 70 μm laser spot, and an average composition was determined (results reported in the appendix). This approach has some drawbacks, particularly regarding zoning of trace elements within individual crystals in carbonate veins. However, this approach was chosen to (a) avoid inclusions within veins (b) minimise sample preparation time and (c) allow veins with complex internal fabrics to be documented more completely. Multiple major and trace elements (^{23}Na, ^{24}Mg, ^{29}Si, ^{43}Ca, ^{44}Ca, ^{45}Sc, ^{49}Mn, ^{57}Fe, ^{85}Rb, ^{88}Sr, ^{89}Y, ^{138}Ba, ^{139}La, ^{140}Ce, ^{141}Pr, ^{146}Nd, ^{147}Sm, ^{153}Eu, ^{158}Gd, ^{163}Dy, ^{166}Er, ^{174}Yb, ^{208}Pb, ^{232}Th, ^{238}U) were simultaneously analysed during laser sampling by repeated, rapid sequential peak hopping, with a mass spectrometer cycle time of 0.65 s. Data reduction followed established protocols for time-resolved analysis (Longerich et al, 1996), with NIST 612 standard (values of Pearce et al, 1997),

analyzed before and after every 6 samples. and ^{43}Ca was used as an internal standard. Laser pulse rates of 5 Hz in combination with a laser fluence of 5 J/cm^2, short laser wavelength (λ= 193 nm), and aperture imaging optics were used to attain controlled calcite ablation (~1 μm per second) in a He ablation medium (Eggins et al, 1998).

Chemical Results

Characterising the isotopic and trace element composition of a heterogeneous host rock is a challenging problem. For example, it is difficult to determine the overall oxygen or strontium isotope composition of a calcareous shale because small variations in the proportion of carbonate:silicate minerals may cause significant changes in Sr or O isotope ratios. In addition, it is not feasible to characterise each individual bed in an interbedded limestone-shale unit, and then produce an 'average' isotopic composition. The majority of veins in the Taemas Vein Swarm are calcite, with minor quartz. Cox (2007) suggested that the silicate-rich Majurgong Formation had no affect on the oxygen isotope composition of fluids migrating through this unit. Therefore, it was decided to characterise

only the *carbonate* component of host rocks via weak acid extraction of carbonate. In particular, extracting only the Rb-poor carbonate component of host rocks means that no age correction is required to determine $^{87}Sr/^{86}Sr$ values at the time of hydrothermal vein growth (Faure and Powell, 1972).

Distal limestone samples (more than 50 metres from significant veining) have $\delta^{18}O$ between 23-25 ‰, $\delta^{13}C$ of -0.5 to +3.0 ‰ (Cox, 2007), and $^{87}Sr/^{86}Sr$ ratios between 0.70815 and 0.70828 (Table 2), which are consistent with seawater values for the middle Devonian (Veizer et al, 1999). Host rocks measured within ~ 1 mm to 1 cm of vein margins have a broader range of $\delta^{18}O$, varying between 14 — 24‰ (Cox, 2007). Depleted $\delta^{18}O$ margins are usually a few centimetres wide, except around a fault zone at the bottom of the Cavan Bluff Limestone (Figure 5), where $\delta^{18}O$ depleted zones are a few metres wide (Cox, 2007). A few veins (< 10) showing significantly lower than host rock $\delta^{13}C$ values (up to -11 ‰). Vein carbonate $\delta^{18}O$ values show significant variation, from ~ 0‰ to 25‰. Vein carbonates $^{87}Sr/^{86}Sr$ vary between 0.70808 and 0.70897,

which are significantly greater than the range of host rock carbonate $^{87}Sr/^{86}Sr$ values. Sr isotope ratios show no systematic relationship to $\delta^{18}O$ (Fig. 8) or $\delta^{13}C$ values.

Oxygen isotope compositions from calcite and quartz inferred to have grown in equilibrium (i.e. intergrown fibrous quartz and calcite) suggest fluid temperatures between 100 and 250 °C (Table 3, Fig. 9; thermometer of Zheng, 1993).

Host rock carbonates have variable Mg concentrations, particularly in the Cavan Bluff Limestone (see Table 4 for host rock carbonate trace element compositions). In general, the CBL has higher concentrations of Mg, Mn, Sc, Y and the rare earth elements (REEs). Strontium concentrations are relatively constant throughout the Murrumbidgee Group (1000-2000 ppm). The massive Currajong and Receptaculites Limestones generally have lower concentrations of most trace elements, in comparison to the interbedded limestone-shale members (Cavan Bluff, Spirifer yassensis and Bloomfield Limestones). Host rock REE, Y and Sc concentrations, and REE patterns are similar to those measured in Devonian limestones by Nothdurft et al (2004).

Carbonate veins have Mn concentrations which are similar to

host limestone carbonate, while Sr concentrations are generally higher than host rock carbonates, particularly for veins within the CBF. Vein carbonate has highly variable Sc, Y and REE concentrations.

Chemical variations in vein composition with stratigraphic position

Vein $\delta^{18}O$ increases with stratigraphic height through the Murrumbidgee Group (Fig. 10). However, variations in vein $\delta^{18}O$ values are seen at any one stratigraphic level, with veins (exceptionally) having ~10‰ $\delta^{18}O$ variation. Veins in the Currajong Limestone have slightly lower $^{87}Sr/^{86}Sr$ ratios than veins in the interbedded limestone-shale units (Fig. 10). Below the Cavan Bluff Limestone, vein carbonate $^{87}Sr/^{86}Sr$ is slightly lower than CBL $^{87}Sr/^{86}Sr$ host rock carbonate compositions. However, within the CBL, vein carbonate is slightly higher, or in equilibrium with the host rock carbonate with respect to $^{87}Sr/^{86}Sr$.

Within the SYL, veins have higher $^{87}Sr/^{86}Sr$ than host rock carbonate. $^{87}Sr/^{86}Sr$ decreases with increasing stratigraphic height towards the Currajong Limestone. Within the CJL, veins are generally in equilibrium with host rock carbonate with respect to

$^{87}Sr/^{86}Sr$. However, veins in the interbedded limestones and shales of the immediately overlying Bloomfield Limestone show $^{87}Sr/^{86}Sr$ values elevated above host rock values.

In the interbedded limestone-shale lithologies, veins have the most variable trace element concentrations, particularly in the Cavan Bluff Limestone (Fig. 11). Generally, trace element concentrations in vein carbonate decrease with increasing stratigraphic height (excepting Mg). Lead concentrations in veins are consistently lower than host rock carbonate. Scandium, Y and heavy REE concentrations are generally similar, or lower than host rock carbonate. Light REE concentrations decrease with increasing stratigraphic height, while the heavy REEs show a more limited concentration decrease with increasing stratigraphic height. Chondrite normalized (values of McDonough and Sun, 1995) REE patterns in Cavan Bluff veins are generally LREE enriched, whereas veins higher in stratigraphy in the SYL and CJL become relatively depleted in LREE.

Chemical variations within and between outcrops

Veins were assessed on an outcrop-by-outcrop, and within-outcrop

scale to examine how fluid-rock reaction varies between veins in a similar host rock. Figure 5 shows the location, vein type and isotopic compositions of different veins (fault, bedding-parallel and extension) from a fold-fault complex in the CBL. Notable is that $\delta^{18}O$ varies by ~ 5‰ and $^{87}Sr/^{86}Sr$ varies between 0.70825 and 0.70846. A small extension vein isolated within a single limestone bed (likely formed during flexural flow folding) shows higher $^{87}Sr/^{86}Sr$ and $\delta^{18}O$, while bedding-parallel and fault veins show some of the lowest $\delta^{18}O$ and $^{87}Sr/^{86}Sr$ ratios.

Figure 12 illustrate the structural setting and Sr and O isotope ratios of veins from an outcrop ('Site A') of folded Spirifer yassensis Limestone, at Kangaroo Flat. This outcrop is immediately adjacent (separated by approximately 50 m horizontally, Fig. 2) from an outcrop (Site 'B') from which the Sr and O isotope composition of veins was also measured (see Barker et al., 2009, their Fig. 2). These outcrops represent one of the few locations in which the chemistry of veins from the same stratigraphic level, but different structural settings may be compared (see highlighted regions in Fig. 4). Site A (Figure 12) has two open, asymmetric folds which contains a larger bedding-parallel vein. Site B is an upright, close fold containing

predominantly bedding-parallel veins, with several small dilational jogs and late bedding-perpendicular extension veins related to limb-parallel stretching.

Within both outcrops, vein carbonate $\delta^{18}O$ varies between 20 and 25‰ for most veins (excepting a late strike-slip fault vein; 14.7 ‰), and vein $\delta^{18}O$ values for the two outcrops are statistically indistinguishable at the 95% confidence level (p-value=0.63, Mann-Whitney test). However, the vein cluster at 'Site A' (Fig. 12) has consistently lower $^{87}Sr/^{86}Sr$ ratios than the 'Site A' vein cluster ($^{87}Sr/^{86}Sr$ p-value=0.016; Fig. 13). These two different vein clusters also have significantly different concentrations of Mn, Fe, Sr and Eu. Veins in the 'Site A' have higher Mn, Fe and Eu concentrations, and lower Sr concentrations (p-values for Mann-Whitney test; Mn=< 0.0001, Fe=< 0.0001, Sr= 0.0009, Eu= 0.0133; Fig. 13). For normalised REE patterns, both outcrops have LREE enriched patterns, with veins in the 'Site A' having a more positive Eu anomaly than veins at 'Site B'.

Vein-type variations

Approximately eighty different bedding-parallel, extension and fault

veins were analyzed from the Spirifer yassensis and Currajong Limestones. Within the SYL, $\delta^{18}O$ in vein carbonate varies between 14.7 and 25.2 ‰, with the majority of veins having $\delta^{18}O$ values between 22 and 25 ‰. Strontium isotope values ($^{87}Sr/^{86}Sr$) show no relationship to the vein type (Fig. 14). Similarly, all veins within the CJL have $\delta^{18}O$ of 20 to 25 ‰, with the majority of values clustering between 22 and 24‰. However, $^{87}Sr/^{86}Sr$ values systematically vary according to vein type, with extension veins having lower $^{87}Sr/^{86}Sr$ values than most fault or bedding-parallel veins (Fig. 14).

Similar trends are observed for trace elements, with veins in the SYL having a broad range of trace element compositions, with no relationship observed between vein type and trace element concentration (Fig. 15). In comparison, extension veins within the CJL have lower concentrations of most trace elements compared to fault or bedding-parallel veins (Fig. 16). In particular, REE concentrations are lower in extension veins than in bedding-parallel or fault veins.

Extension veins in the Currajong Limestone have Sr isotope and trace element compositions that are most similar to host rock carbonate compositions. In comparison, all veins in the SYL have a

broad range of Sr isotope ratios and trace element concentrations, which are generally elevated above host rock carbonate compositions. Many extension veins in the CJL are related to fold limb-parallel stretching. In comparison, most extension veins in the Spirifer yassensis Limestone are associated with bedding-discordant fault zones. The fluid which migrated through late extension veins in the CJL may have undergone significantly more fluid-rock reaction with the local host rock than the fluid from which fault or bedding-parallel veins formed.

Discussion

Stable and radiogenic isotopic composition of vein calcite

If it is assumed that calcite precipitated in equilibrium with the parent fluid, and the fluid temperature can be estimated, then the $\delta^{18}O$ of vein calcite may be used to determine the isotopic composition of the parent fluid. Quartz-calcite oxygen isotope pairs (see Fig. 10, and Cox, 2007), suggest fluid temperatures of 100-250 ^{o}C, with the presence of illite implying temperatures of < 200 °C (Cox, 2007). Minimum $\delta^{18}O$ values measured in veins at the base of the Cavan Bluff Limestone are ~0 to + 2‰ (Cox, 2007). At

temperatures of 100-200 °C, this implies that fluid $\delta^{18}O$ was between -14 ‰ and -8 ‰ (Zheng, 1999). Such low $\delta^{18}O$ values are consistent with a meteoric fluid source (Sheppard, 1986). To form a meteoric fluid with these low $\delta^{18}O$ values, the meteoric fluid must have been sourced at either high latitude (~50 to 60º), or significant altitude (2-4 km; Bowen and Wilkinson, 2002).

Several veins, or sections of individual veins have unusually elevated $^{87}Sr/^{86}Sr$ and $\delta^{13}C$ values *(e.g.* sample C2a, see appendix). Barker et al (2006) and Cox (2007) attributed localised negative-$\delta^{13}C$ values to oxidation of organic matter during fluid-rock reaction. The coupling of elevated $^{87}Sr/^{86}Sr$ and depleted $\delta^{18}O$ values implies that a second fluid 'source' may have been present. This fluid may have been a residual interstitial pore fluid, which underwent enhanced fluid-rock reaction with iron oxides (causing oxidation of organic carbon) and ^{87}Sr-enriched clay minerals (i.e. dominant Majurgong Formation, SYL) prior to mixing with the invading meteoric fluid.

Assuming that calcite-deposition in veins was an equilibrium process, then the $\delta^{18}O$ of vein carbonate changes in response to the $\delta^{18}O$ of pore fluid, as pore fluid and wall rock undergo progressive

reaction. These results emphasise that veins within the same outcrop may have considerably different isotopic compositions (compare vein pair 1 and 3, and vein pair 6 and 7 in Fig. 7). Variations in the isotopic composition of veins within the same outcrop indicate that fluids which precipitated calcite in fault and bedding-parallel veins underwent less interaction with host rocks than extension veins. This is likely related to the length of fluid-flow pathways, with fault and bedding-parallel veins having (relatively) short flow pathways, causing fluids to undergo less reaction with host rock.

Variations in $^{87}Sr/^{86}Sr$ are not consistent with fluids only reacting with host rock carbonate. Sr isotope ratios in veins measured near the base of the Cavan Bluff Limestone have $^{87}Sr/^{86}Sr$ ratios only slightly below host rock carbonate values, with most veins in the CBL being in equilibrium with host rock carbonate with respect to $^{87}Sr/^{86}Sr$. However, in the SYL, $^{87}Sr/^{86}Sr$ ratios are substantially higher than host rock values. This is attributed to reaction of fluids with minerals that have higher concentrations of radiogenic ^{87}Sr in the Majurgong Formation, and shale-rich layers of the Spirifer yassensis Limestone.

The transition from the SYL to CJL is marked by a change between

mixed shale-limestone lithology to only limestone, and a decrease in vein $^{87}Sr/^{86}Sr$. Carbonate contents of SYL limestone determined in the laboratory (estimated from loss of weight after acetic acid leaching) are 85-90% carbonate, while CJL limestones are 97-98% carbonate. The decrease in $^{87}Sr/^{86}Sr$ from the SYL to the CJL is interpreted to be a result of decreasing amounts of shale being available for fluid-rock reaction (i.e. increasing amounts of carbonate to buffer fluids). Carbonate veins in the Bloomfield Limestone (interbedded limestone-shale) have $^{87}Sr/^{86}Sr$ values elevated significantly above host rock carbonate, even as little as ~10 m stratigraphically above the Currajong Limestone. This implies that fluids strip trace elements from the surface of clays and other minerals over short reactive path lengths during fluid flow.

Trace elements in paleohydrothermal systems

In this section, trace element variations between veins in different stratigraphic units are discussed. During this study a relatively low number of host rocks were analyzed. In particular, analyses of shales were avoided during this study. This decision was made due to (a) the paucity of fresh shale in outcrop and (b) logistical problems of

characterising hundreds to thousands of individual sedimentary horizons. The consistent isotopic and trace element compositions of limestone carbonate throughout the stratigraphic sequence suggests that average carbonate compositions do not vary by a significant degree (except perhaps for Mg), particularly compared to the degree of variation in trace element concentrations in veins. The study of Cox (2007) demonstrated that fluids dominantly interacted with carbonate with respect to $\delta^{18}O$. Thus, comparing only vein calcite with only host rock carbonate minerals allows other controls on vein chemistry (such as interaction with other minerals, changes in physiochemical conditions) to be assessed.

Trace element concentrations in hydrothermal calcite veins may be affected by several factors, including:

(1) Spatial and temporal variations in the composition of infiltrating (source) fluid.

(2) Interaction of source fluid with matrix fluid.

(3) Dissolution of host rock minerals, releasing lattice-bound trace and minor elements *i.e.* host carbonate being dissolved.

(4) Scavenging by fluids of trace elements loosely bound to

mineral surfaces, particularly for clays, releasing adsorbed elements.

(5) Precipitation of hydrothermal minerals *(e.g.* calcite) leading to coprecipitation of other trace elements, removing those elements from solution.

(6) Sorption of trace elements onto mineral surfaces during fluid migration, removing trace elements from fluids.

(7) Changes in physiochemical conditions *(e.g.* temperature, pressure, pH, complexing species), which may affect trace element incorporation and fractionation from fluids.

Use of different isotope systems provides insights into different fluid-rock reaction processes. For example, fluids infiltrating the bottom of the Murrumbidgee Group precipitated veins with extremely depleted oxygen isotope values relative to host rock carbonate. However, these same fluids precipitated veins which are essentially host rock-buffered with respect to $^{87}Sr/^{86}Sr$. These differences reflect the rate of different fluid-mineral reactions, and the different partition coefficients between rock and fluid for different elements.

Steefel and Lichtner (1998) and DePaolo (2006) provide models

addressing the chemical interaction of host rock, ‘matrix fluid’ and ‘fracture fluid’ during fracture-controlled fluid flow. As fluid migrates through a fracture, diffusion of trace elements occurs between that fluid, and the rock matrix. The position of alteration fronts will be dependent on the fluid flow rate, diffusion rate, kinetics of reactions, and reactive surface area of minerals. Along any one fracture, these three factors will change depending on the fracture aperture, fracture roughness and wall rock composition. For example, a small cataclastic fault zone, containing pulverised host rock with a high reactive surface area, will react in a different manner to a smooth sided extension fracture cutting through the same host rock.

To understand causes of trace-element variations in an exhumed hydrothermal system, it is necessary to characterise the host rock mineralogy, the chemistry and surface reactivity of those minerals, and the chemistry of both ‘matrix fluid’ and ‘fracture fluid’. This may be possible in a modern hydrothermal system such as a mid-ocean ridge, with relatively simple, homogeneous host rock (basalt) and homogeneous, well-characterised fluid (sea water). However, it is not possible in an exhumed, ancient hydrothermal system with a

diverse mineralogy and fluids with unconstrained composition. Thus, discussion in this section is largely qualitative, aimed towards understanding what processes may control trace element variations within hydrothermal systems.

Trace element concentrations in vein carbonate are considerably higher than host rock carbonate for most elements in the Cavan Bluff Limestone. This implies that the fluid which invaded the base of the Murrumbidgee Group was already enriched in trace elements. Presumably, the trace element composition of fluids infiltrating the base of the CBF reflects fluid-rock interaction which occurred with underlying rocks (i.e. volcanic sediments of the Black Range Group). Notable in some veins within the Cavan Bluff Limestone are elevated Sr concentrations, and veins with extremely positive Eu anomalies, which could be produced by dissolution of Ca-feldspar, which has appreciable concentrations of both Sr and Eu (Schnetzler and Philpotts, 1970).

When vein REE concentrations are normalised to chondrite values, it is apparent that REE patterns in Cavan Bluff veins are generally LREE enriched, whereas veins higher in stratigraphy in the SYL and CJL become gradually depleted in LREE. In hydrothermal fluids,

REE fractionation is a function of (a) sorption and desorption of REEs during migration of fluids along particle surfaces and (b) coprecipitation (Bau and Moller, 1992). Carbonate and hydroxyl ligands form stronger complexes with HREEs than LREEs (Bau and Moller, 1992). In carbonate-dominated hydrothermal solutions (such as those which would be expected in limestones), calcite precipitating from solutions with relatively low CO_3^{2-} concentrations will have flatter chondrite normalised REE patterns than calcite precipitating from a solution with higher CO_3^{2-} concentrations, which will be relatively enriched in the LREEs. This is because in carbonate-poor solutions there will be little difference in the complexing of the light and heavy REEs (Bau, 1991; Bau and Moller, 1992). If this interpretation is correct, it is suggested that $[CO_3^{2-}]$ decreased as fluids migrated upwards through the Murrumbidgee Group. Such a change would be consistent with decreasing fluid pressure, as fluids ascended upwards.

Development of bedding-parallel veins during fold growth

It is suggested that crack-seal layers developed in bedding-parallel veins were developed by multiple, low magnitude earthquakes

during flexural slip fold growth. The separation of crack-seal bands within these BPV may be used to infer some characteristics of the earthquake slip events which formed the bands. If a dilational jog opens perpendicular to the finite slip vector on a fault plane, then the width of the resulting dilational jog (parallel to the finite slip vector) is equal to the displacement along the fault plane. Crack-seal bands in laminated BPV typically have separations of 0.1 mm to 2 mm (thus implying earthquake displacements of 0.1 to 2 mm).

The typical ratio of average displacement (u) to fault rupture length (L) for an earthquake lies between 10^{-5} and 10^{-4} (Wells and Coppersmith, 1994). If this scaling relationship holds for the seismic events which are inferred to produce the crack-seal bands in these laminated veins, then fault displacements of 0.1 to 2 mm imply fault rupture lengths of 1 metre to 200 metres, and rupture areas (assuming that rupture area is $\sim L^2$) of ~ 1 m to 40,000 m (Sibson, 2001). These would be equivalent to earthquake moment magnitudes of approximately 0 to +2 (Sibson, 2001), or possibly magnitudes as high as +4 (Wells and Coppersmith, 1994). These calculations gives a rough estimate of the length of fluid flow pathways generated along bedding-parallel veins during seismic slip,

assuming that permeability was significantly enhanced along fault rupture planes following earthquake slip (Sibson, 2001). Larger earthquake ruptures along bedding-parallel veins may have occurred, but no information on the dimensions of these ruptures is texturally preserved in the resulting veins.

Implications for fluid flow pathways and vein development during crustal shortening

Important conclusions that may be drawn from this study, and the previous studies of Barker et al (2006) and Cox (2007) are:

(1) Veins formed over an extended period, from early during folding until after fold lock-up and cleavage development.

(2) Depleted $\delta^{18}O$ ratios in vein carbonate relative to host rock carbonate indicate that fluid was derived externally to the host rocks.

(3) Reactive transport modelling of oxygen isotope variations by Cox (2007) demonstrate that the systematic increase in vein $\delta^{18}O$, and marked O-isotope alteration front in the Taemas Vein Swarm was the result of the buffering of an infiltrating low-$\delta^{18}O$ fluid by progressive fluid-rock reaction, with fluid flow largely restricted to fractures with no substantial lateral fluid

flow into vein sidewalls.

(4) Analyses of vein $\delta^{18}O$ and $^{87}Sr/^{86}Sr$ conducted during this study, and results reported in Barker et al (2006) and Cox (2007) reveal that fluid flow pathways, path lengths and/or fluid flow and fluid-rock reaction rates changed dynamically during the growth of individual veins, and between different veins in the same outcrop. This is likely related to the creation and destruction of permeability during repeated fracture opening and sealing events.

Dynamic switches in fluid flow pathways could be interpreted in terms of fluid flow through a fault-fracture mesh (Hill, 1977; Sibson, 2001). In such a mesh, it is predicted that fractures will be transiently permeable after fracturing (promoting rapid migration of fluids), and then this permeability will be destroyed (i.e. via hydrothermal mineral deposition), thus creating a dynamic fluid flow environment.

According to the conditions for tensile failure, fluid pressure must exceed the least compressive stress and the tensile strength of the rock to cause extension fractures to form. In a contractional (i.e. reverse) faulting regime, gently dipping extension veins imply that

(a) the least compressive stress was approximately vertical and (b) that the fluid pressure (at least transiently) exceeded the lithostatic pressure (i.e. $\lambda_v > 1.0$; Sibson, 2001). Additional evidence for transiently high fluid pressures is provided by steeply dipping bedding-parallel slip veins, and severly misoriented bedding-discordant faults. The presence of folded and unfolded laminations in some of these veins suggests that slip continued on these veins throughout fold growth, with some vein dips exceeding 70°. For slip to continue at severe misorientation requires that fluid pressures exceed supralithostatic levels (Sibson, 1985).

Timing relationships between bedding-parallel slip veins and overprinting flexural flow and extension veins, indicate that early during folding, fluids migrated along bedding surfaces, probably after small, bedding-parallel slip events (i.e. microearthquakes). Later in folding, once fold lock-up occurred, fluid flow may have occurred along bedding-discordant faults and extension vein networks associated with fold limb stretching, rather than being isolated along bedding planes.

Differential stress levels must have varied significantly during deformation (at least on a local scale). Parts of the stratigraphy must

have had low differential stress levels at the time of vein formation to form extension fractures. Mutually overprinting relationships between shear and extension fractures indicate that differential stress values oscillated between $(\sigma_1 - \sigma_3) < 4T$ and $(\sigma_1 - \sigma_3) > 5.66T$, where T is the tensile strength of the rock (Hancock, 1985). Such differential stress variations could be related to stress loading and release during repeated seismic slip events (Sibson, 1989), during progressive fold growth and crustal shortening.

Generally, fluid flow in fracture-controlled hydrothermal systems is expected to be discontinuous, with breaches of overpressured fluid reservoirs by fault rupture allowing the ascent of over-pressured fluids (Cox, 2005). During each breach of an overpressured reservoir, a fluid pressure pulse will migrate upwards, and be preferentially transmitted along the more permeable, recently ruptured fault zone. The fluid pressure increase will begin to diffuse into the surrounding rocks, potentially causing a cascade of failure on other faults (i.e. aftershocks), and also leading to the tensile failure criterion to be met, causing extension fracturing (Fitzenz and Miller, 2001; Miller, 2002; Miller et al, 2004). This will in turn generate further permeability as fault slip and fracturing occur.

In active fold-and-thrust belts, strain is accommodated in sedimentary rocks by a combination of folding and thrust faulting *(e.g.* Shaw and Suppe, 1994). Seismic reflection profiles and surface mapping suggest that actively growing folds are intimately related to seismically active faults (e.g. Namson and Davis, 1988; Davis et al., 1989; Shaw and Suppe, 1994). It is inferred that fold growth in many sedimentary sequences involves flexural slip folding, particularly early in fold growth, prior to lockup of fold limbs (Ramsay, 1974). Crack-seal textures in bedding-parallel veins at Taemas indicate that bedding-parallel slip was episodic, suggesting that fold growth occurred episodically. Episodic fold growth and associated faulting would likely generate significant fracture permeability in actively deforming fold-thrust belts (Finkbeiner et al, 1997).

In reservoir-related seismicity from the Nurek Reservoir, Vakhsh valley, Tadjikistan, a series of small earthquakes (magnitudes -0.5 to +2) occurred above a major thrust sheet, in folded sedimentary rocks overlying a larger thrust fault at depths of 0 to 8 km. The focal mechanisms for these earthquakes showed maximum compression perpendicular to fold axes mapped at the surface (Keith et al, 1982; Leith and Simpson, 1986). However, none of these earthquakes

could be correlated with larger faults mapped at the surface. This implies that the microseismicity must have been restricted to small faults (e.g. fault lengths of less than 5 km), related to active fold growth. This earthquake sequence appears similar in tectonic setting and perhaps slightly larger, or similar in scale to bedding-parallel slip seismicity inferred for the Taemas Vein Swarm.

Conclusions

The Taemas Vein Swarm preserves evidence for hydrothermal vein growth during fold growth. Vein formation was intimately related to space created during folding, with vein growth active from the early to the latest stages of fold growth. Mutually crosscutting relationships between veins indicate that vein growth was intermittent, and that veins formed as localised stress fields underwent significant changes in both orientation and magnitude.

Subhorizontal extension fractures and severly misoriented faults indicate that fluid pressures intermittently exceeded lithostatic levels, over (at least) local regions of the deforming crust. Individual veins grew incrementally, and preserve a variety of

textures (fibrous, massive and laminated), and indicate that vein opening and mineral deposition rates varied significantly. Mutually crosscutting veins, and incrementally developed vein textures imply that high-permeability fluid flow pathways varied dynamically through time and space.

The isotopic and trace element composition of syntectonic veins reflect different degrees of fluid-rock reaction during hydrothermal fluid flow. Strontium isotope ratios ($^{87}Sr/^{86}Sr$) indicate that fluids react with host rock carbonate, but also scavenge Sr from Sr-enriched minerals *(e.g.* illite), within shale beds over short reactive path lengths. Trace element concentrations generally decrease with increasing stratigraphic height. Rare earth element concentrations and patterns are influenced by progressive calcite precipitation and sorption along fluid-flow pathways, and changes in REE complexation in solution.

A progressive increase in vein $\delta^{18}O$ with increasing height through the Murrumbidgee Group is attributed to progressive buffering of ^{18}O-depleted fluids by reaction with host rock carbonate. Vein $\delta^{18}O$ values imply that the invading fluid had $\delta^{18}O$ compositions consistent with a meteoric fluid source. The isotopic

and trace element compositions of hydrothermal veins is variable across stratigraphy, between outcrops, within individual outcrops and within individual hydrothermal veins (Barker et al., 2006). Variability in O and Sr isotope ratios within and between veins is attributed to variable fluid-rock reaction along dynamically changing fluid flow pathways, caused by episodic fracturing and fluid flow events accompanying seismicity within a fault-fracture mesh.

Vein growth is inferred to be closely linked to seismic activity. Understanding the timing and growth of fluid flow networks during folding has implications for the localisation of ore mineralisation, and the trapping of hydrocarbons in fold structures.

References

Abart R, Pozzorini D (2000) Implications of kinetically controlled mineral-fluid exchange on the geometry of stable-isotope fronts. European Journal of Mineralogy 12:1069–1082

Abart R, Sperb R (1997) Grain-scale stable isotope disequilibrium during fluid-rock interaction. 1: Series approximations for

advective-dispersive transport and first-order kinetic mineral-fluid exchange. American Journal of Science 297:679–706

Badertscher N, Abart R, Burkhard M, McCaig A (2002) Fluid flow pathways along the Glarus Overthrust derived from stable and Sr-isotope patterns. American Journal of Science 302:517–547

Barker S, Cox S, Eggins S, Gagan M (2006) Microchemical evidence for episodic growth of antitaxial veins during fracture-controlled fluid flow. Earth and Planetary Science Letters 250:331–344

Barker S, Bennett C, Cox S, Norman D, Gagan M (2009) Sm-Nd, Sr, C and O isotope systematics in hydrothermal calcite-fluorite veins: implications for fluid-rock reaction and geochronology. Checmial Geology 268: 58-66

Bau M (1991) Rare-earth element mobility during hydrothermal and metamorphic fluid-rock interaction and the significance of the oxidation state of europium. Chemical Geology 93:219–230

Bau M, Moller P (1992) Rare earth element fractionation in metamorphogenic hydrothermal calcite, magnesite and siderite. Mineralogy and Petrology 45:231–246

Bickle M, McKenzie D (1987) The transport of heat and matter by fluids during metamorphism. Contributions to Mineralogy and

Petrology 95:384–392

Bowen G, Wilkinson B (2002) Spatial distribution of $\delta^{18}O$ in meteoric precipitation. Geology 30:315–318

Bowman J, Willett S, Cook S (1994) Oxygen isotopic transport and exchange during fluid flow: one-dimensional models and applications. American Journal of Science 294:1–55

Browne I (1958) Stratigraphy and structure of the Devonian rocks of the Taemas and Cavan areas, Murrumbidgee River, south of Yass, N.S.W. Journal and Proceedings of the Royal Society of New South Wales 4:115–128

Coplen T, Kendall C, Hopple J (1983) Comparison of stable isotope reference samples. Nature 302:236–239

Cox S (2005) Coupling between deformation, fluid pressures and fluid flow in ore-producing hydrothermal systems at depth in the crust. Economic Geology and the Bulletin of the Society of Economic Geologists 100:39–75

Cox SF (2007) Structural and isotopic constraints on fluid flow regimes and fluid pathways during upper crustal deformation: an example from the Taemas area of the Lachlan Orogen, south-eastern Australia. Journal of Geophysical Research

112:doi:10.1029/2006JB004,734

Cramsie J, Pogson D, Baker C (1975) Yass 1:100,000 Geological Sheet 8628. Geological Survey of New South Wales, Sydney

Davis, T.L., Namson, J., and Yerkes, R.F., 1989, A cross section of the Los Angeles area; seismically active fold and thrust belt, the 1987 Whittier Narrows earthquake, and earth- quake hazard: Journal of Geophysical Research, v. 94, p. 9644–9664.

DePaolo D (2006) Isotopic effects in fracture-dominated reactive fluid-rock systems. Geochimica et Cosmochimica Acta 70:1077–1096

DePaolo D, Getty S (1996) Models of isotopic exchange in reactive fluid-rock systems: implications for geochronology in metamorphic rock. Geochimica et Cosmochimica Acta 60:3933–3947

Dietrich D, McKenzie J, Song H (1983) Origin of calcite in syntectonic veins as determined from carbon-isotope ratios. Geology 11:547–551

Eggins S, Kinsley L, Shelley J (1998) Deposition and element fractionation processes during atmospheric pressure laser sampling for analysis by ICP-MS. Applied Surface Science 127-129:278–

Eggins S, Grun R, McCulloch MT, Pike AW, Chappell J, Kinsley L, Mortimer G, Shelley M, Murray-Wallace CV, Spotl C, Taylor L (2005) In situ U-series dating by laser-ablation multi-collector ICPMS: new prospects for Quaternary geochronology. Quaternary Science Reviews 24:2523–2538

Eppel H, Abart R (1997) Grain-scale stable isotope disequilibrium during fluid-rock interaction; 2, an example from the Penninic-Austroalpin tectonic contact in eastern Switzerland. American Journal of Science 297:707–728

Faure G, Powell J (1972) Strontium isotope geology. Springer, New York

Finkbeiner T, Barton C, Zoback M (1997) Relationships among in-situ stress, fractures and faults, and fluid flow: Monterey formation, Santa Maria basin, California. American Association of Petroleum Geologists 81:1975–1999

Fitzenz D, Miller S (2001) A forward model for earthquake generation on interacting faults including tectonics, fluids, and stress transfer. Journal of Geophysical Research 106:26,689–26,706

Fowler T (1996) Flexural-slip generated bedding-parallel veins from

central Victoria, Australia. Journal of Structural Geology 18:1399–1415

Gaviglio P (1986) Crack-seal mechanism in a limestone; a factor of deformation in strike-slip faulting. Tectonophysics 131:247–255

Gerdes M, Baumgartner L, Person M (1995) One- and two-dimensional models of fluid flow and stable isotope exchange at an outcrop in the Adamello contact aureole, Southern Alps, Italy. American Mineralogist 80:1004–1019

Glen R (1992) Thrust, extensional and strike-slip tectonics in an evolving Palaeozoic orogen; a structural synthesis of the Lachlan Orogen of southeastern Australia. Tectonophysics 214; 1-4:341–380

Hancock P (1985) Brittle microtectonics: principles and practice. Journal of Structural Geology 7: 4378-457

Hill D (1977) A model for earthquake swarms. Journal of Geophysical Research 82:1347-1352

Jessell M, Willman C, Gray D (1994) Bedding parallel veins and their relationship to folding. Journal of Structural Geology 16:753–767

Keith C, Simpson D, Soboleva O (1982) Induced seismicity and

style of deformation at Nurek Reservoir, Tadjik, USSR. Journal of Geophysical Research 87:4609–4624

Knoop S, Kennedy L, Dipple G (2002) New evidence for syntectonic fluid migration across the hinterland-foreland transition of the Canadian Cordillera. Journal of Geophysical Research-Solid Earth 107: doi:10.1029/2001JB000217

Koehn D, Passchier C (2000) Shear sense indicators in striped bedding-veins. Journal of Structural Geology 22:1141–1151

Lassey K, Blattner P (1988) Kinetically-controlled oxygen isotope exchange between fluid and rock in one-dimensional advective flow. Geochimica et Cosmochimica Acta 52:2169–2175

Leith W, Simpson D (1986) Seismic domains within the Gissar-Kokshal Seismic Zone, Soviet Central Asia. Journal of Geophysical Research 91:689–699

Longerich H, Jackson S, Gunter D (1996) Laser ablation inductively coupled plasma mass spectrometric transient signal data acquisition and analyte concentration calculation. Journal of Analytical Atomic Spectrometry 11:899–904

McDonough W, Sun S (1995) The composition of the Earth. Chemical Geology 120:223-253

Matthaei S (2003) Fluid flow and (reactive) transport in fractured and faulted rock. Journal of Geochemical Exploration 78-79:179–182

McCaig A, Wayne D, Marshall J, Banks D, Henderson I (1995) Isotopic and fluid inclusion studies of fluid movement along the Gavarnie Thrust, Central Pyrenees - reaction fronts in carbonate mylonites. American Journal of Science 295:309–343

McCaig A, Wayne D, Rosenbaum J (2000) Fluid expulsion and dilatancy pumping during thrusting in the Pyreness: Pb and Sr isotope evidence. Geological Society of America Bulletin 112:1199–1208

Miller S (2002) Properties of large ruptures and the dynamical influence of fluids on earthquakes and faulting. Journal of Geophysical Research 107:doi:10.1029/2000JB000,032

Miller S, Collettini C, Chiaraluce L, Cocco M, Barchi M, Kaus B (2004) Aftershocks driven by a high-pressure CO_2 source at depth. Nature 472:724–727

Mueller W, Aerden D, Halliday A (2000) Isotopic dating of strain fringes. Science 288:2195–2198

Namson, J.S. and Davis, T.L. (1988) Seismically active fold and

thrust belt in the San Joaquin Valley, Central California. Geological Society of America Bulletin v. 100:257-273

Nothdurft L, Webb G, Kamber B (2004) Rare earth element geochemistry of Late Devonian reefal carbonates, Canning Basin, Western Australia: Confirmation of a seawater REE proxy in ancient limestones. Geochimica et Cosmochimica Acta 68:263–283

Pearce N, Perkins W, Westgate J, Gordon M, Jackson S, Neal C, Chenery S (1997) A compilation of new and published major and trace element data for the NIST SRM 610 and NIST SRM 612 glass reference materials. Geostandards and Geoanalytical Research 21:115-144

Pfiffner O, Ramsay J (1982) Constraints on geological strain rates: arguments from finite strains in naturally deformed rocks. Journal of Geophysical Research 87:311– 321

Ramos FC, Wolff JA, Tollstrup DL (2004) Measuring $^{87}Sr/^{87}Sr$ variations in minerals and groundmass from basalts using LA-MC-ICPMS. Chemical Geology 211:135–158

Ramsay J (1974) Development of chevron folds. Geological Society of America Bulletin 85:1741–1753

Ramsay JG, Huber M (1987) The techniques of modern structural

geology. Volume 2: Folds and Fracture. Academic Press, London

Rye D, Bradbury H (1988) Fluid flow in the crust: an example from a Pyrenean thrust ramp. American Journal of Science 288:197–235

Schnetzler CC, Philpotts JA (1970) Partition coefficients of rare-earth elements between igneous matrix material and rock-forming mineral phenocrysts - II. Geochimica et Cosmochimica Acta 34:331–340

Sharp Z (1990) A laser-based microanalytical method for the in situ determination of oxygen isotope ratios of silicates and oxides. Geochimica et Cosmochimica Acta 54:1353–1357

Shaw J, Suppe J (1994) Active faulting and growth folding in the eastern Santa Barbara Channel, California. Geological Society of America Bulletin 106:607–626

Sheppard S (1986) Characterization and isotopic variations in natural waters. In: Valley J, Taylor J HP, O'Neil J (eds) Stable isotopes in high temperature geological processes, Reviews in Mineralogy, vol 16, Mineralogical Society of America, Chelsea, MI, pp 165–183

Sibson R (1985) A note on fault reactivation. Journal of Structural Geology 7:751–754

Sibson R (1989) Earthquake faulting as a structural process. Journal of Structural Geology 11:1–14

Sibson R (2001) Seismogenic framework for hydrothermal transport and ore deposition. In: Structural controls on ore genesis, Reviews in Economic Geology, vol 14, Society of Economic Geologists, Boulder, pp 25–50

Steefel C, Lichtner P (1998) Multicomponent reactive transport in discrete fractures: I. Controls on reaction front geometry. Journal of Hydrology 209:186–199

Steefel C, DePaolo D, Lichtner P (2005) Reactive transport modelling: an essential tool and a new research approach for the Earth sciences. Earth and Planetary Science Letters 240:539–558

Tanner P (1989) The flexural-slip mechanism. Journal of Structural Geology 11:635– 655

Tesoriero A, Pankow J (1996) Solid solution partitioning of Sr^{2+} , Ba^{2+} , and Cd^{2+} to calcite. Geochimica et Cosmochimica Acta 60:1053–1063

Veizer J, Ala D, Azmy K, Bruckschen P, Buhl D, Bruhn F, Carden G, Diener A, Ebneth S, Godderis Y, Jasper T, Korte G, Pawellek F, Podlaha O, Strauss H (1999) $^{87}Sr/^{86}Sr$, $\delta^{13}C$ and $\delta^{18}O$ evolution

of Phanerozoic seawater. Chemical Geology 161(1-3):59–88

Wells D, Coppersmith K (1994) New empirical relationships among magnitude, rupture length, rupture width, rupture area and surface displacement. Bulletin of the Seismological Society of America 84:974–1002

Woodhead J, Swearer S, Hergt J, Maas R (2005) In situ Sr-isotope analysis of carbonates by LA-MC-ICP-MS: interference corrections, high spatial resolution and an example from otolith studies. Journal of Analytical Atomic Spectrometry 20:22–27

Zack T, John T (2007) An evaluation of reactive fluid flow and trace element mobility in subducting slabs. Chemical Geology 237:5–22

Zheng Y (1993) Calculation of oxygen isotope fractionation in anhydrous silicate minerals. Geochimica et Cosmochimica Acta 57:1079–1091

Zheng Y (1999) Oxygen isotope fractionation in carbonate and sulfate minerals. Geo-chemical Journal 33:109–126

Table 1 (see next page): Stratigraphy and brief description of host rocks for the Taemas Vein Swarm. Note the abbreviations for host rocks used in the text. See Browne (1958) and Cramsie et al (1975) for further details.

Table 2 Host rock carbonate Sr isotope ratios (and associated errors) as measured by TIMS.

Sample	$^{87}Sr/^{86}Sr$	$\pm 2\sigma$
Cavan Bluff Host Rock 1	0.70828	0.00003
Cavan Bluff Host Rock 2	0.70828	0.00002
Spirifer Yassensis Host Rock 1	0.70826	0.00003
Spirifer Yassensis Host Rock 2	0.70826	0.00001
Currajong Host Rock 1	0.70821	0.00002
Currajong Host Rock 2	0.70815	0.00003
Bloomfield Host Rock 1	0.70825	0.00002
Bloomfield Host Rock 2	0.70826	0.00003
Receptaculites Host Rock 1	0.70821	0.00002
Receptaculites Host Rock 2	0.70819	0.00001

Table 3 Oxygen isotope ratios ($\delta^{18}O$, VSMOW) for coexisting quartz and calcite fibres from two different samples.

Sample	Qtz $\delta^{18}O_{(VSMOW)}$	Cct $\delta^{18}O_{(VSMOW)}$
CL12-7	26.8	24.1

CL12-5	27.1	23.8
CL12-4	25.8	24.0
Cjcrk-C3	26.0	23.8
Cjcrk-C4	26.1	23.8
Cjcrk-C5	26.9	23.9
Cjcrk-C6	27.1	23.8
Cjcrk-C7	26.9	25.0
Cjcrk-Jl	27.1	23.9
Cjcrk-J2	25.5	23.9
Cjcrk-Ka	26.1	23.6
Cjcrk-Kb	27.1	23.6

Table 4 Host rock carbonate trace element composition for selected trace elements (concentrations given in parts per million, ppm). Cavan Bluff Limestone = CBHR; Spirifer Yassensis Limestone = SP1 and SP2; Currajong Limestone = CJ1 and CJ2; Bloomfield Limestone = BL1 and BL2; Receptaculites Limestone = RCP1 and RCP2.

Elemen	CBHR	CBHR	SP1	SP2	CJ1	CJ2	BL1	BL2	RCP1	RCP2
Mg	57783	9767	7165	4931	3395	5821	2526	1921	2529	1848
Sc	4.29	2.67	1.47	1.59	0.61	0.40	1.72	1.50	1.28	0.90
Mn	1026	821	312	118	63	47	284	476	154	160
Fe	1264	1805	2500	3500	2105	2014	2326	2183	1848	1593
Rb	1.10	0.54	0.60	0.63	0.13	0.15	0.63	0.52	0.50	0.42
Sr	1556	1478	1123	1647	1078	2182	1805	1808	1057	910
Y	20.13	19.34	5.77	3.86	2.40	1.09	5.31	6.17	2.93	2.36

Ba	39.21	38.13	10.21	8.18	6.10	6.61	9.51	8.70	6.81	5.81
La	16.86	19.43	5.43	3.93	1.46	1.00	4.94	4.18	3.10	2.25
Ce	37.63	42.39	12.33	8.95	3.33	1.98	11.17	10.56	6.71	4.93
Pr	4.04	4.48	1.51	1.12	0.36	0.21	1.46	1.47	0.79	0.59
Nd	16.99	18.08	6.19	4.57	1.48	0.84	6.19	6.70	3.19	2.36
Sm	4.02	3.94	1.32	0.91	0.33	0.19	1.27	1.50	0.62	0.47
Eu	0.98	0.89	0.29	0.20	0.08	0.04	0.36	0.62	0.16	0.11
Gd	4.17	4.01	1.26	0.83	0.38	0.18	1.16	1.38	0.58	0.45
Tb	0.65	0.61	0.19	0.12	0.06	0.03	0.17	0.20	0.09	0.07
Dy	3.88	3.55	1.09	0.69	0.37	0.17	0.97	1.12	0.50	0.41
Ho	0.77	0.70	0.21	0.13	0.08	0.04	0.20	0.21	0.10	0.08
Er	2.03	1.83	0.54	0.35	0.21	0.09	0.49	0.51	0.27	0.21
Yb	1.69	1.40	0.42	0.30	0.18	0.08	0.41	0.37	0.21	0.18
Lu	0.23	0.20	0.06	0.04	0.03	0.01	0.06	0.05	0.03	0.02
Pb	3.79	2.81	1.23	0.89	0.75	0.24	1.06	1.26	0.66	0.62
Th	1.24	1.56	0.62	0.83	0.31	0.15	0.71	0.89	0.34	0.25
U	0.38	0.64	1.99	1.38	1.51	0.75	0.49	0.24	0.62	1.12

Fig. 1 Schematic diagrams showing evolution of vein $\delta^{18}O$ compositions with time and space during progressive fluid-rock reaction (modified after Cox, 2007). (a) Fluid from a fluid reservoir with a depleted ^{18}O composition advects through a rock sequence with a less depleted ^{18}O composition. (b) Evolution of vein $\delta^{18}O$ compositions with time (t_0, t_1, t_2, t_3) as low $\delta^{18}O$ advect through the rock mass. (c) Illustration of how a vein at the same distance along a fluid flow pathway could have a markedly different $\delta^{18}O$ composition depending on the fluid flow and/or reaction rate between rock and fluid. (d) Evolution of the $\delta^{18}O$ composition of a vein with time at a single point 'α' in (a), depending on the fluid-rock reaction rate. With a more rapid reaction rate, fluid becomes more more rapidly buffered by the host rock carbonate.

Fig. 2 Simplified geological map of the Taemas Peninsula (modified from Cox, 2007), showing representative bedding orientations, and major outcrop locations documented in this paper. Map grid is Australian Geodetic Datum (1984). Figures 4, 5, 7, 13 and 14 are at 1ocation 1, Figure 6 is from location 2. Other locations are noted in text. Cross sections (a-a'; b-b', c-c', d-d', e-e') are shown in Figure 3.

Fig. 3 Cross sections constructed from field mapping, aerial photographs and pre-dawn infrared images, showing fold style in the Black Range and Murrumbidgee Groups. Note that fold wavelengths are longer (~km scale) in the Black Range Group, and rapidly decrease

to wavelengths of 100 m or less in the Spirifer Yassensis and Bloomfield members of the Taemas Limestone. For clarity, some units which do not crop out are not shown on sections. Equal area stereonet shows poles to bedding (circles) and cleavage (squares) throughout the Taemas Peninsula. Plotted is a best fit great circle, indicating a NNW-SSE trend for the Taemas Synclinorium, with a very gentle south plunge.

Fig. 4 Folded Spirifer Yassensis and Currajong Limestone beds at Kangaroo Flat (Locality 1 on Fig 2). Note decoupling that must occur between and within SYL and CJL limestones to allow observed fold shapes geometries. Black rectangles (from right to left) mark the locations of Figure 6, Site B (see Barker et al., 2009, their Figure 2) and Site A (Figure 12).

Fig. 5 Faults and veins within the Cavan Bluff Limestone at a fault-fold complex at Location 2 on Fig. 2. White lines mark bedding, black lines mark faults. A heavily qtz-cct mineralised fault zone is marked in grey. Shown are O and Sr isotope compositions for different vein types (numbered below) contained within the outcrop: (1) bed-parallel Vein, (2) bed-parallel Vein, (3) saddle-reef, (4) hinge extn vein, (5) flex flow extn vein, (6) laminated fault vein, (7) fault vein dilatant jog. Inset graph shows relationship between $\delta^{18}O$ and $^{87}Sr/^{86}Sr$ for different veins.

Fig. 6 (a) Photograph of Currajong Limestone with extension veins in

subvertical bedding at ‘Kangaroo Flat’ on the eastern side of Taemas Peninsula. (6) Interpretative sketch of (a). Bedding is dashed black, calcite veins are grey. Representative fault and bedding orientations are shown. Equal area stereonet shows the average orientation of bedding (great circle) and poles to veins (note higher density of veins at approximately 90° to bedding). Outcrop is ~ 10 m wide. (c) Photograph of calcite extension veins from limestone on right hand side of photograph (a). Pencil tip (10 cm) for scale. *(d)* Interpretative sketch of (c). Note that vein sets (v_n and v_x) with similar orientations show mutually overprinting relations. Styolites are approximately parallel to bedding. Some veins crosscut styolites, while other veins are truncated against stylolites. (e) Boudinaged limestone beds and extension veins on upper transition of CJL to BFL. Note pencil (15 cm) for scale.

Fig. 7 Schematic diagram showing the growth mechanism and resulting microstructures during the formation of inclusion and crack-seal bands during bedding-parallel slip. Crack-seal bands and layers are produced in dilational jogs, while inclusion bands are produced on the shear planes along which slip is occurring. After Koehn and Passchier (2000).

Fig. 8 Graph of Sr versus oxygen isotope compositions for veins in different stratigraphic units. Striped box represents the compositional range of host rock carbonate.

Fig. 9 Quartz-calcite oxygen isotope pairs ($\delta^{18}O$, relative to VSMOW) plotted on temperature contours derived from (Zheng, 1993). Black squares are data from Cox (2007), open squares are data from this study

Fig. 10 Host rock carbonate (grey data points) and vein carbonate (black symbols) (a) $\delta^{18}O$ and (b) $^{87}Sr/^{86}Sr$; as a function of stratigraphic height through the Murrumbidgee Group. Host rock and open symbols for (a) are from Cox (2007), filled symbols are from this study.

Fig. 11 Mg, Mn, Fe, Sr, Y, La, Ce, Nd, Sm, Eu, Gd and Yb concentrations in host rock carbonate (grey squares), plotted as the range determined for the two samples analyzed from each limestone member (see Table 3), and carbonate veins (black circles) with stratigraphic height through the Murrumbidgee Group (see appendix B). Limestone formations and members are the same as Fig. 11.

Fig. 12 Photo panorama and interpretative sketch showing a bedding-parallel vein and other faults at 'Kangaroo Flat' on the eastern side of Taemas Peninsula (Locality 1 on Fig. 2, Site B). Outcrop is approximately 40 m wide. Bedding traces are dashed lines, and a dolomitic marker bed is shown as hatched grey. The faults are solid black lines, and regions of calcite mineralisation are thicker zones of solid black. Note decoupled bedding and associated wing crack (bottom of sketch). Note that the $\delta^{18}O$ and $^{87}Sr/^{86}Sr$ compositions of specific veins are marked.

Fig. 13 Comparison of $\delta^{18}O$ and $^{87}Sr/^{86}Sr$, and Sr, Eu, Mn and Fe concentrations for two vein clusters at the same stratigraphic level in the Spirifer yassensis Limestone (see also Figs. 4, 5, 13).

Fig. 14 $\delta^{18}O$ and $^{87}Sr/^{86}Sr$ isotope composition of extension, bedding-parallel and fault vein in the Currajong and Spirifer Yassensis Limestones. 2 SE error bars are shown for Sr isotope analyses.

Fig. 15 Trace element composition of extension (grey squares), bedding-parallel (black circles) and fault veins (black diamonds) in the Spirifer yassensis Limestone. Host rock labels show the range of host rock compositions determined

Fig. 16 Trace element composition of extension (grey squares), bedding-parallel (black circles) and fault veins (black diamonds) in the Currajong Limestone.

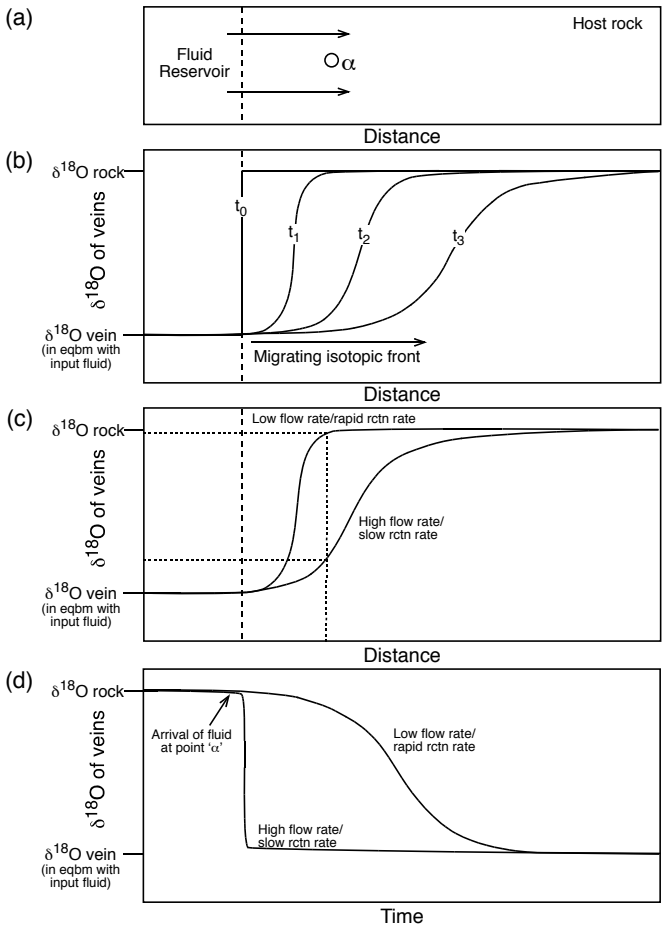
(a)
Host rock
Fluid Reservoir
α
Distance
(b)
δ18O rock
δ18O of veins
t0
t1
t2
t3
δ18O vein (in eqbm with input fluid)
Migrating isotopic front
Distance
(c)
δ18O rock
Low flow rate/rapid rctn rate
δ18O of veins
High flow rate/ slow rctn rate
δ18O vein (in eqbm with input fluid)
Distance
(d)
δ18O rock
Arrival of fluid at point 'α'
Low flow rate/ rapid rctn rate
δ18O of veins
High flow rate/ slow rctn rate
δ18O vein (in eqbm with input fluid)
Time

Figure 1

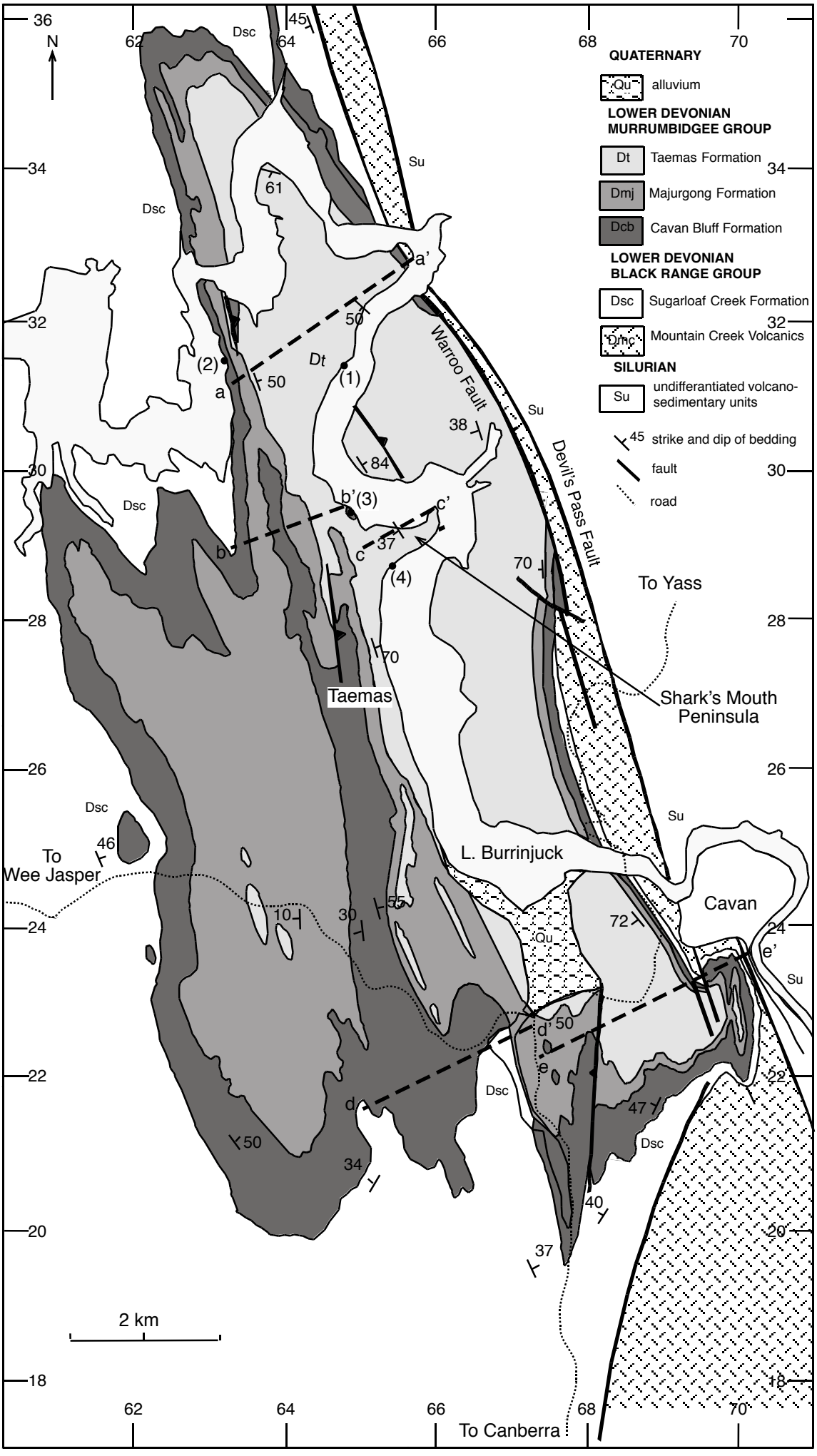
N
QUATERNARY
Qu alluvium
LOWER DEVONIAN
MURRUMBIDGEE GROUP
Dt Taemas Formation
Dmj Majurgong Formation
Dcb Cavan Bluff Formation
LOWER DEVONIAN
BLACK RANGE GROUP
Dsc Sugarloaf Creek Formation
Dmc Mountain Creek Volcanics
SILURIAN
Su undifferantiated volcano-sedimentary units
45 strike and dip of bedding
fault
road
Warroo Fault
Devil's Pass Fault
Taemas
To Yass
Shark's Mouth Peninsula
L. Burrinjuck
Cavan
To Wee Jasper
To Canberra
2 km
a
a'
b
b'
c
c'
d
d'
e
e'
(1)
(2)
(3)
(4)
Dt
Dsc
Su
Qu

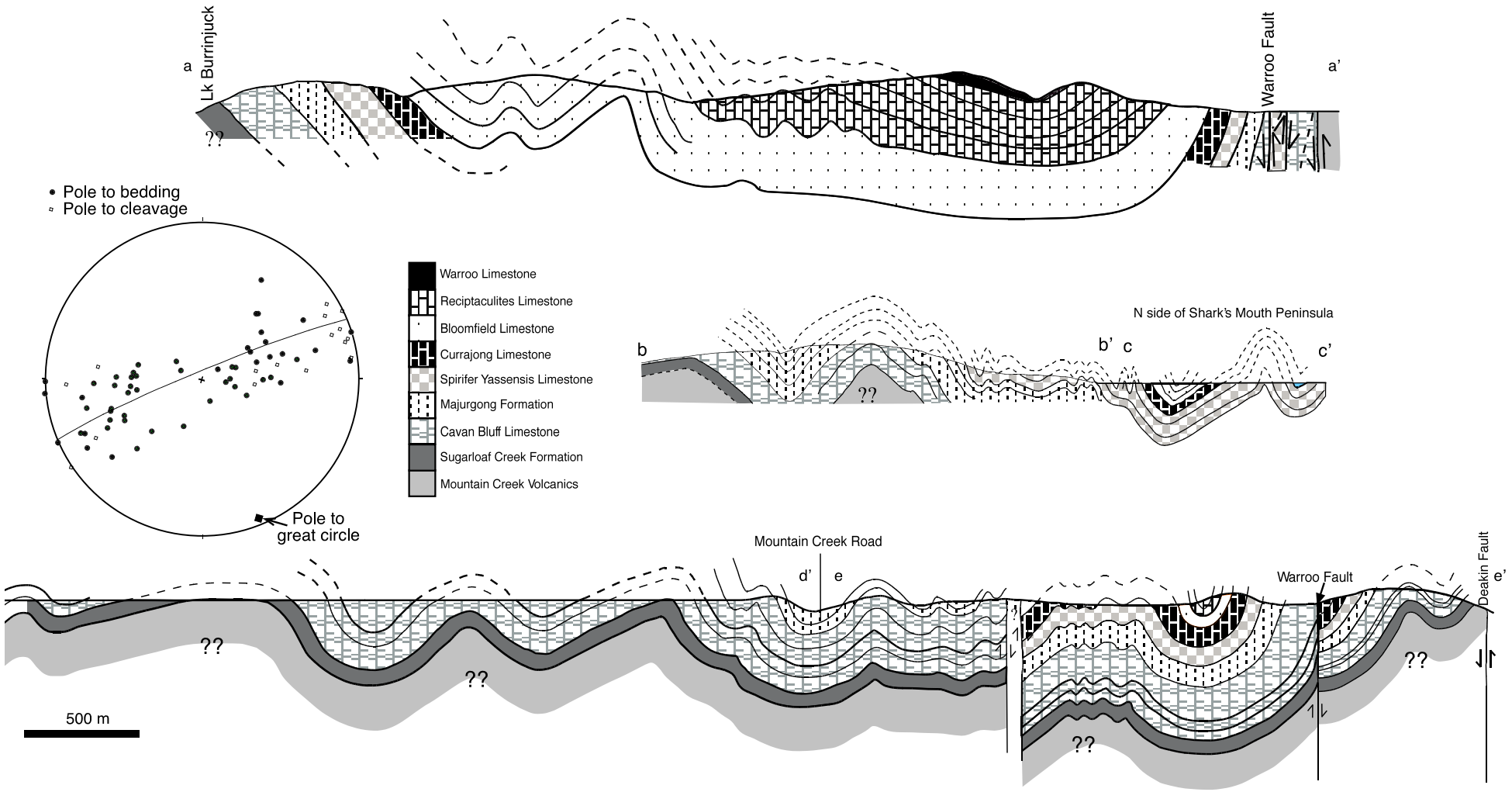
a
Lk Burrinjuck
??
Warroo Fault
a'
• Pole to bedding
▫ Pole to cleavage
Pole to great circle
Warroo Limestone
Reciptaculites Limestone
Bloomfield Limestone
Currajong Limestone
Spirifer Yassensis Limestone
Majurgong Formation
Cavan Bluff Limestone
Sugarloaf Creek Formation
Mountain Creek Volcanics
b
??
b' c
N side of Shark's Mouth Peninsula
c'
Mountain Creek Road
d' e
Warroo Fault
Deakin Fault
e'
??
??
??
??
500 m

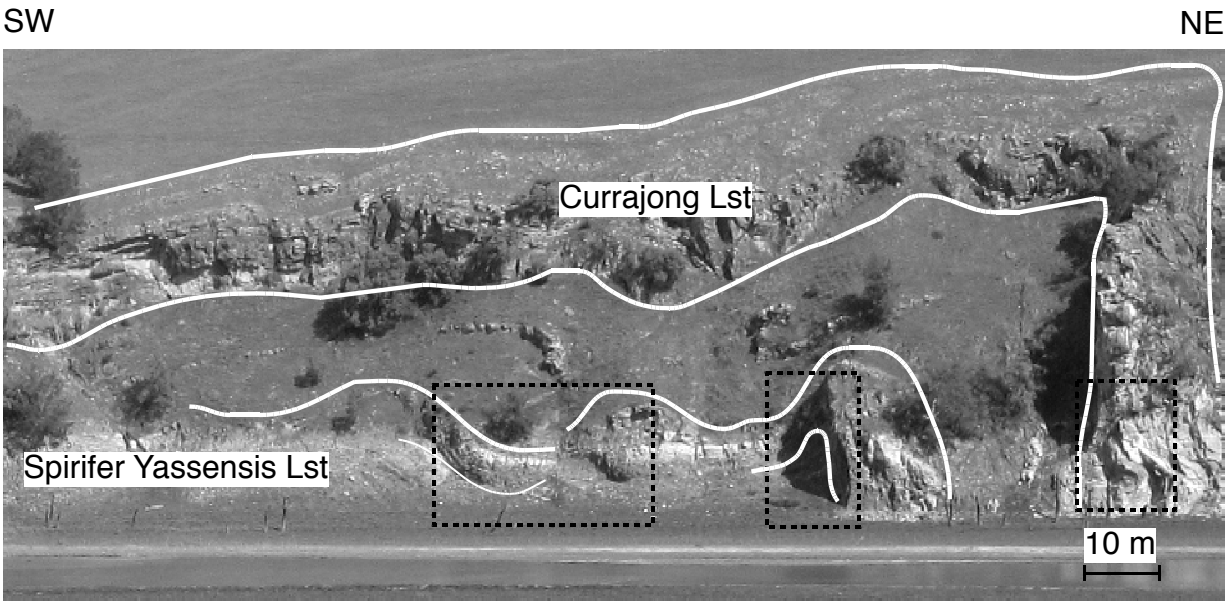

Figure 4

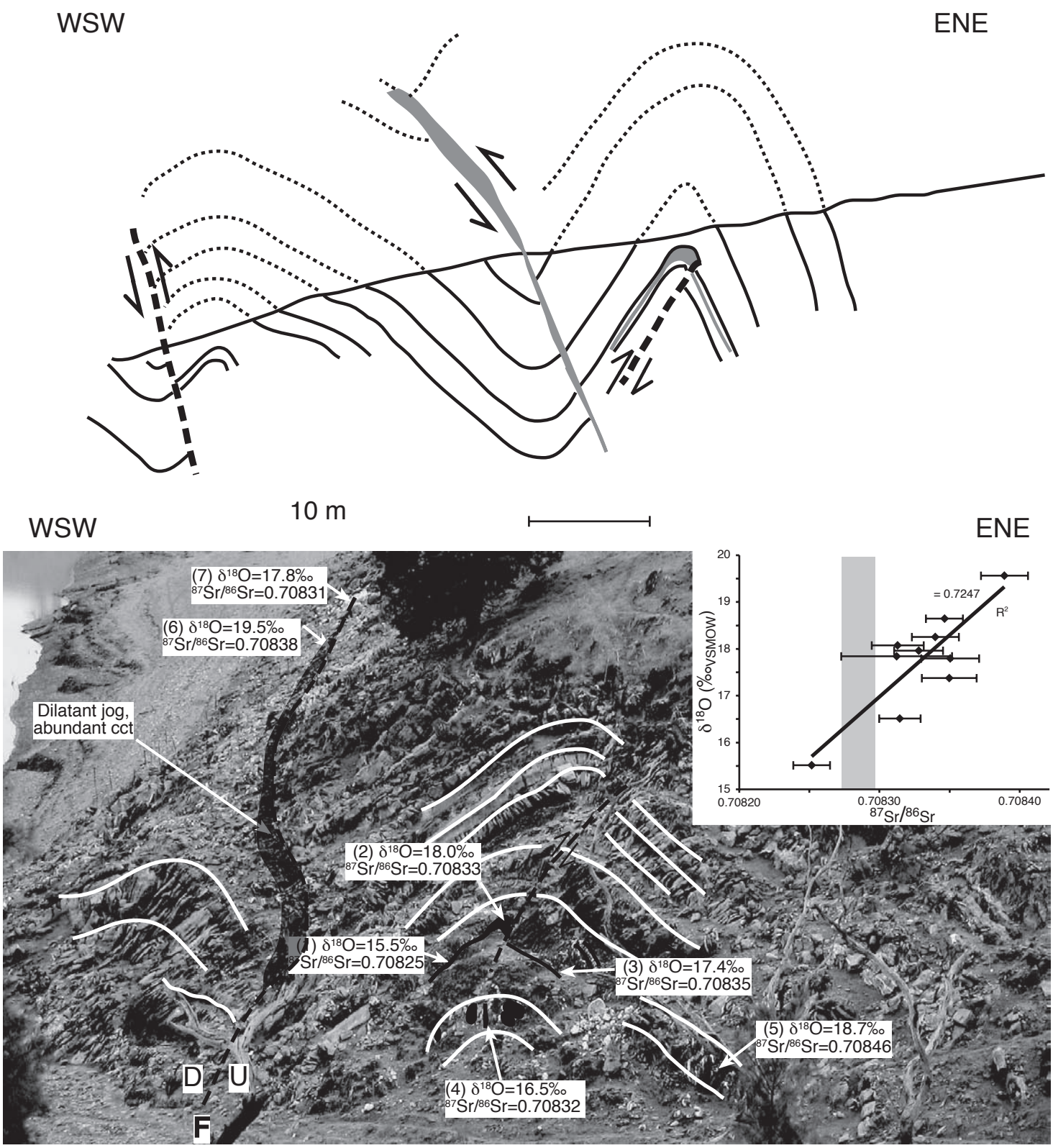
WSW
ENE
10 m
WSW
ENE
(7) δ18O=17.8‰
87Sr/86Sr=0.70831
(6) δ18O=19.5‰
87Sr/86Sr=0.70838
Dilatant jog,
abundant cct
(2) δ18O=18.0‰
87Sr/86Sr=0.70833
(1) δ18O=15.5‰
87Sr/86Sr=0.70825
(3) δ18O=17.4‰
87Sr/86Sr=0.70835
(5) δ18O=18.7‰
87Sr/86Sr=0.70846
(4) δ18O=16.5‰
87Sr/86Sr=0.70832
D
U
F
20
19
18
17
16
15
δ18O (‰VSMOW)
0.70820
0.70830
0.70840
87Sr/86Sr
= 0.7247
R2

Figure 6

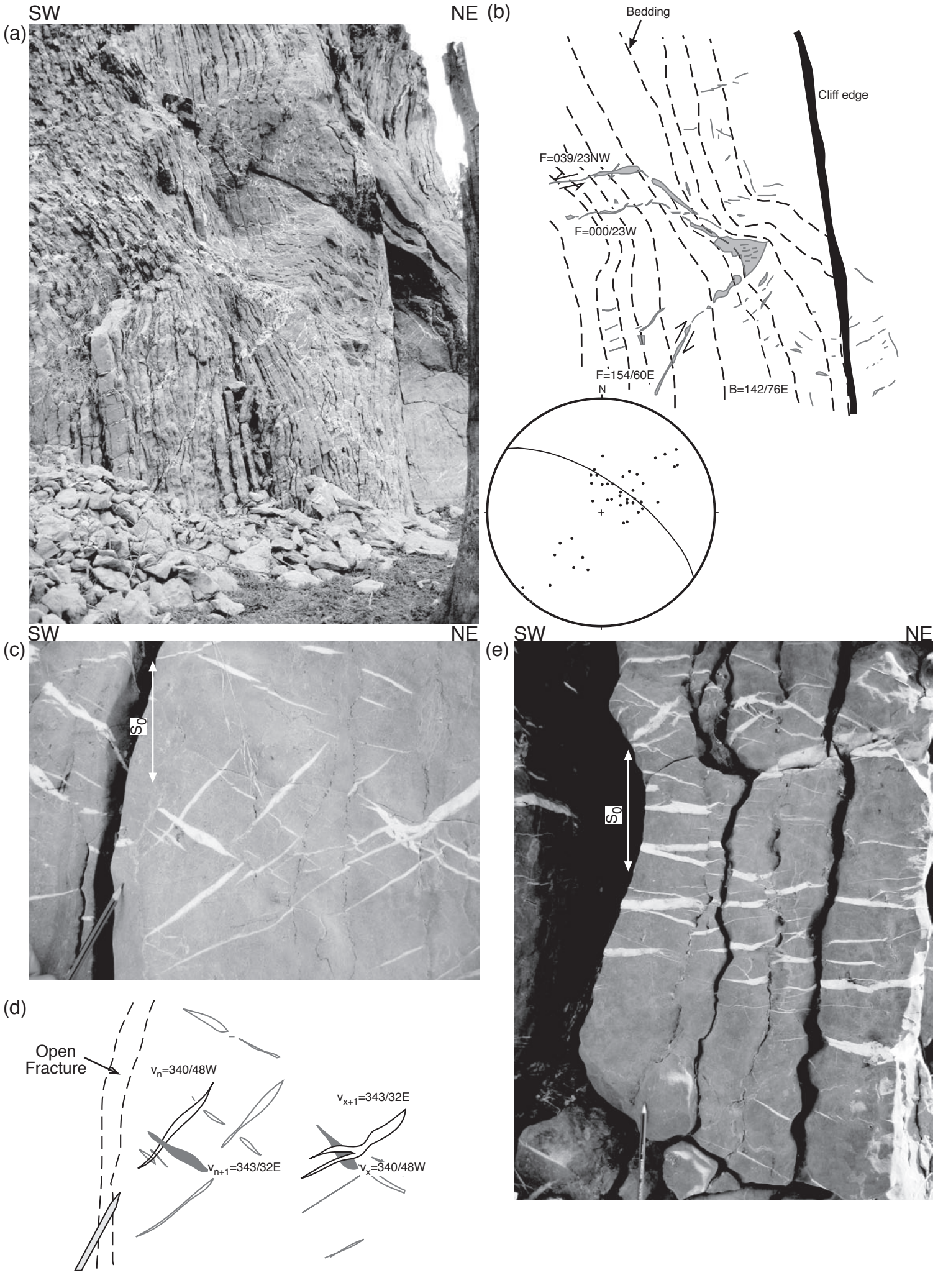
SW
NE
(a)
(b)
Bedding
Cliff edge
F=039/23NW
F=000/23W
F=154/60E
B=142/76E
N
(c)
SW
NE
S0
(d)
Open Fracture
vn=340/48W
vn+1=343/32E
vx+1=343/32E
vx=340/48W
(e)
SW
NE
S0

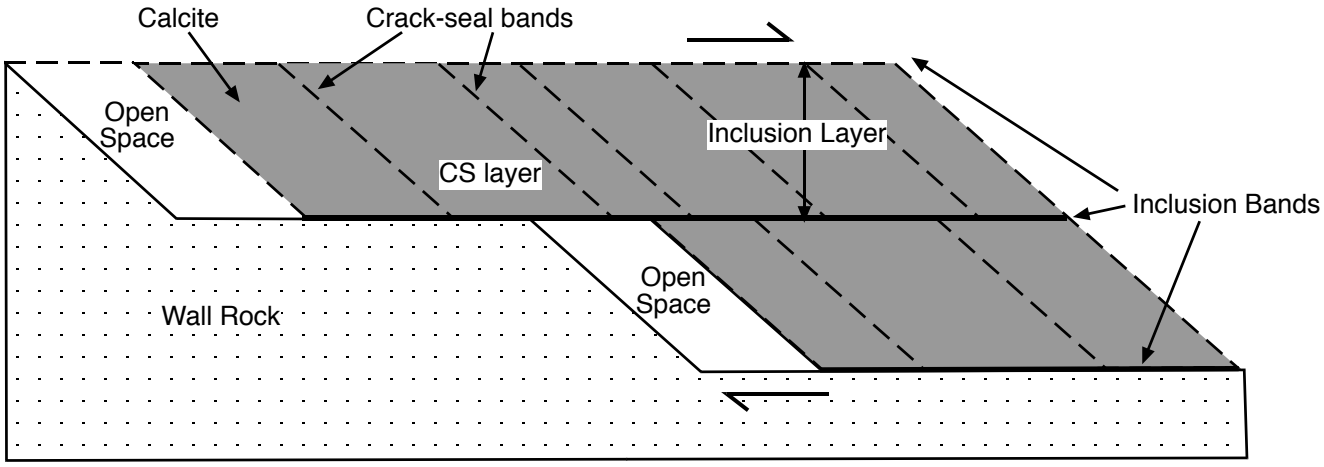
Calcite
Crack-seal bands
Open
Space
CS layer
Inclusion Layer
Inclusion Bands
Open
Space
Wall Rock

Figure 7

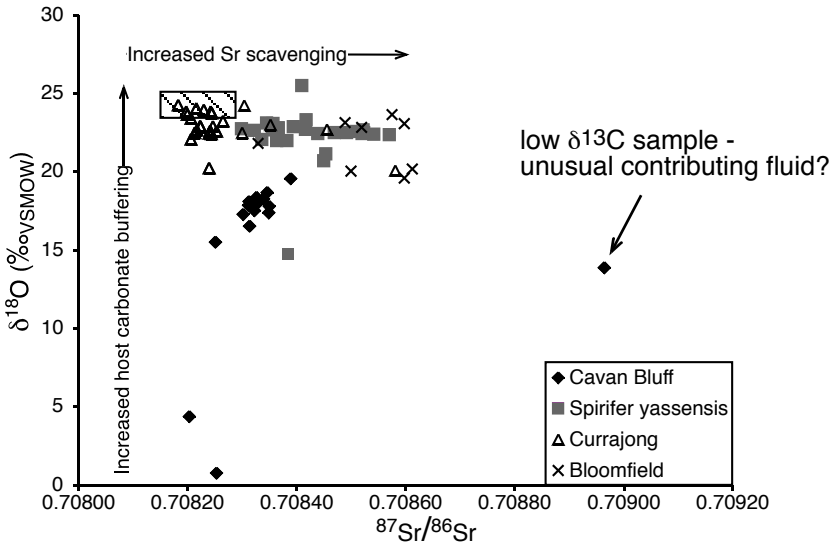
Increased Sr scavenging
Increased host carbonate buffering
low δ13C sample -
unusual contributing fluid?
δ18O (‰VSMOW)
87Sr/86Sr
30
25
20
15
10
5
0
0.70800
0.70820
0.70840
0.70860
0.70880
0.70900
0.70920
Cavan Bluff
Spirifer yassensis
Currajong
Bloomfield

Figure 8

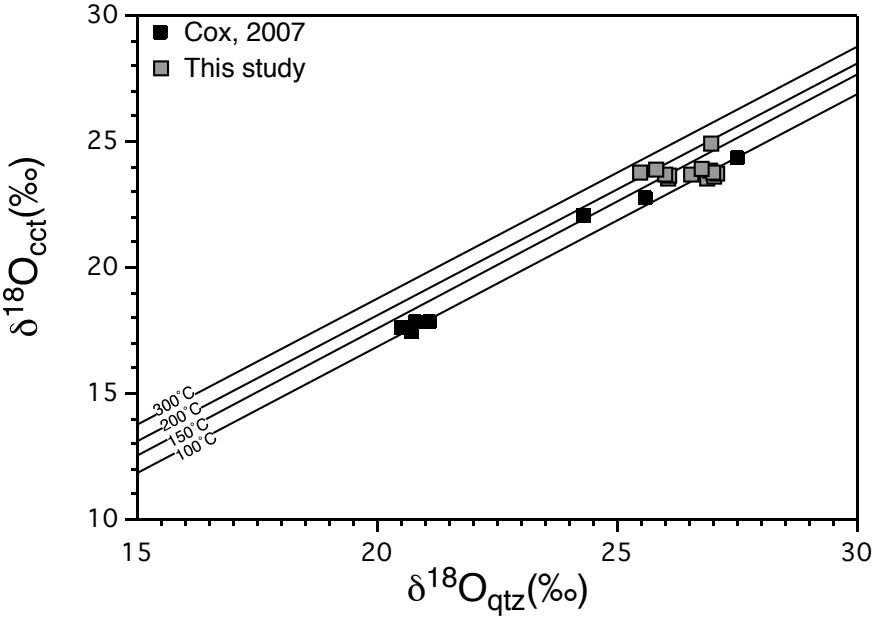
Cox, 2007
This study
300°C
200°C
150°C
100°C
30
25
20
15
10
15
20
25
30
δ18Occt(‰)
δ18Oqtz(‰)

Figure 9

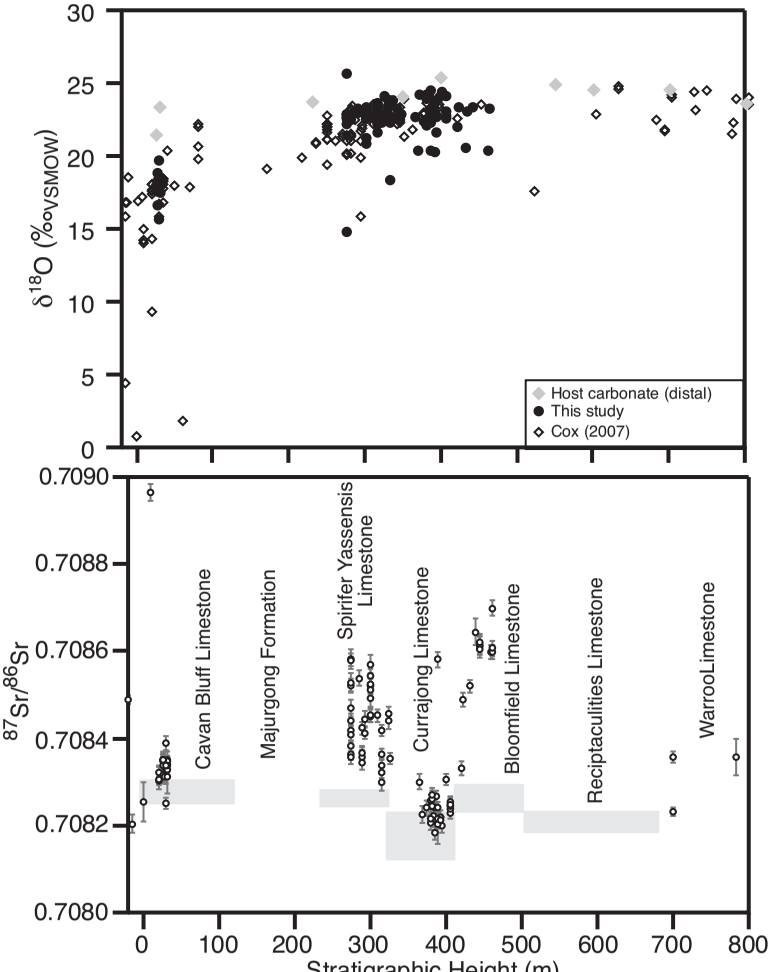
30
25
20
15
10
5
0
δ18O (‰vSMOW)
Host carbonate (distal)
This study
Cox (2007)
0.7090
0.7088
0.7086
0.7084
0.7082
0.7080
87Sr/86Sr
Cavan Bluff Limestone
Majurgong Formation
Spirifer Yassensis Limestone
Currajong Limestone
Bloomfield Limestone
Reciptaculities Limestone
WarrooLimestone
0
100
200
300
400
500
600
700
800
Stratigraphic Height (m)

Figure 11

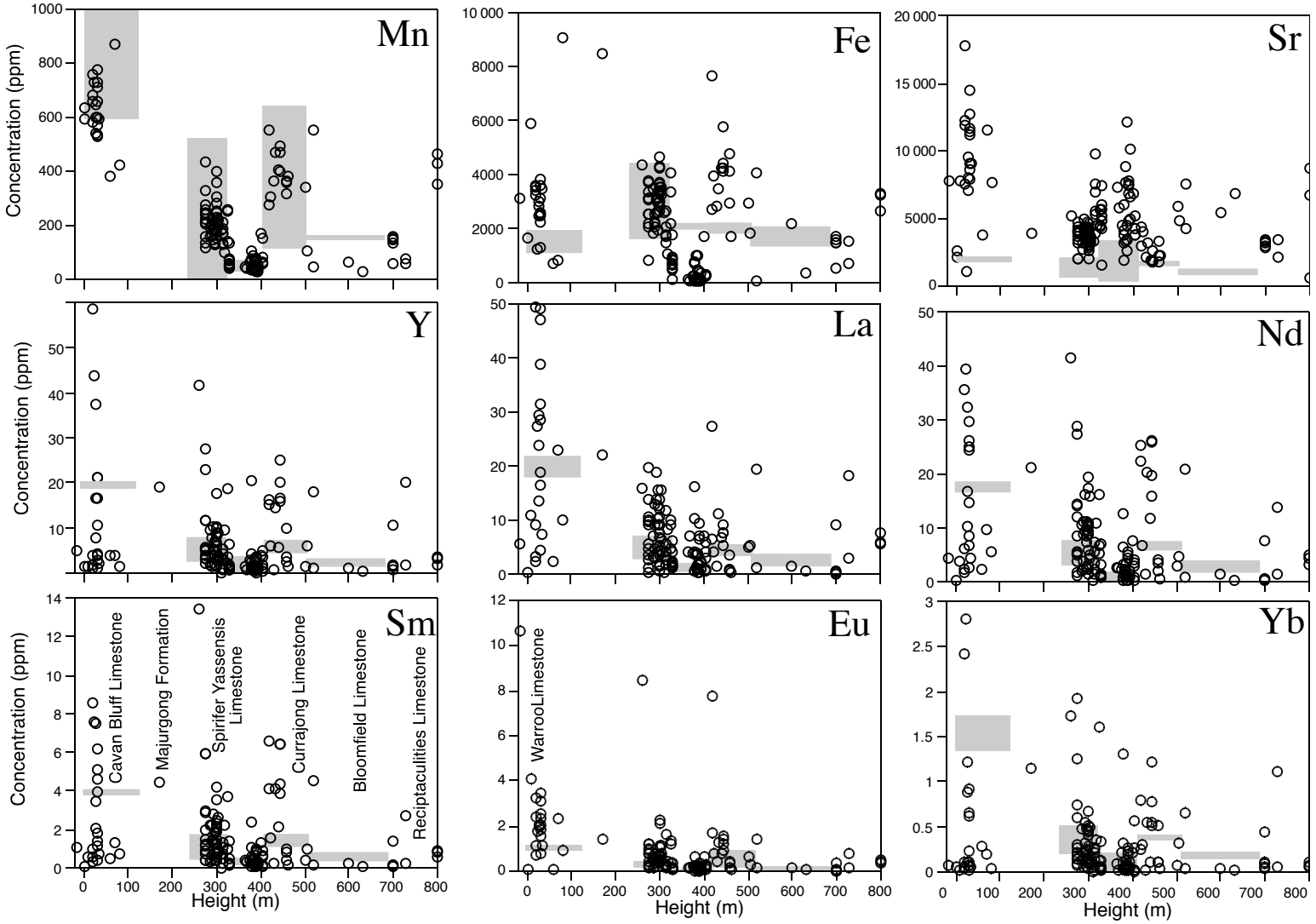
Mn
Fe
Sr
Y
La
Nd
Sm
Eu
Yb
Concentration (ppm)
Height (m)
Cavan Bluff Limestone
Majurgong Formation
Spirifer Yassensis Limestone
Currajong Limestone
Bloomfield Limestone
Reciptaculities Limestone
WarrooLimestone

Figure 11

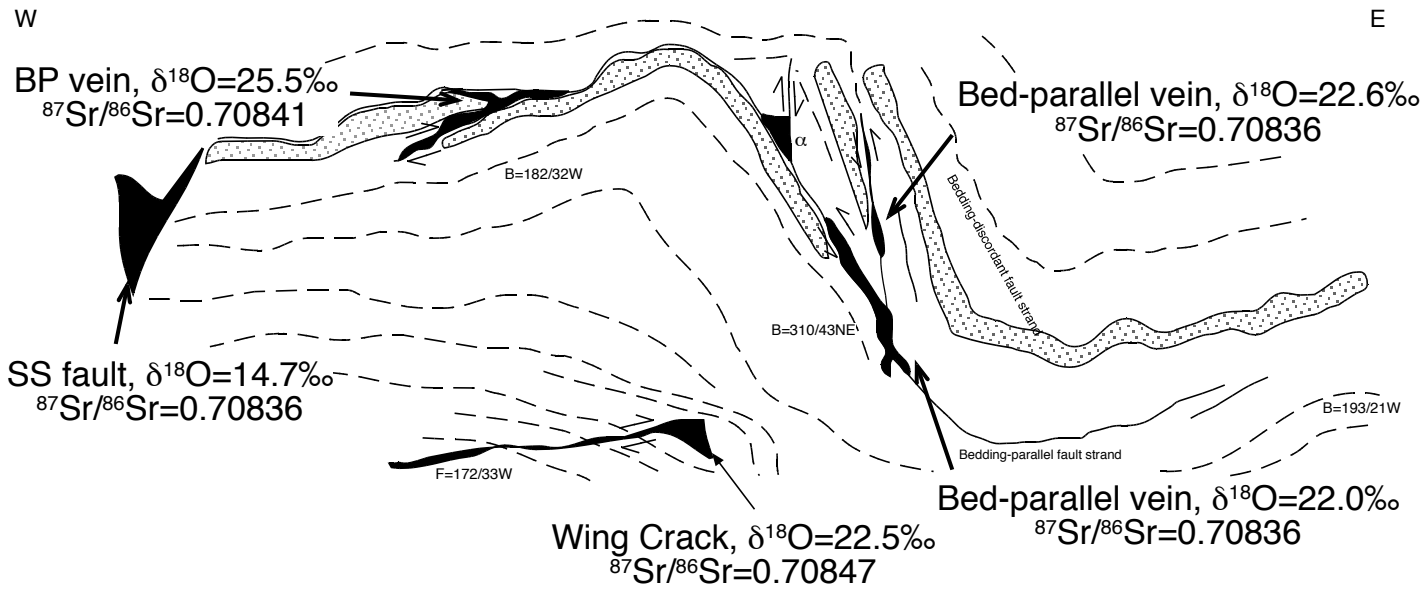
W
E
BP vein, δ18O=25.5‰
87Sr/86Sr=0.70841
B=182/32W
α
Bed-parallel vein, δ18O=22.6‰
87Sr/86Sr=0.70836
Bedding-discordant fault strand
B=310/43NE
SS fault, δ18O=14.7‰
87Sr/86Sr=0.70836
B=193/21W
Bedding-parallel fault strand
F=172/33W
Bed-parallel vein, δ18O=22.0‰
87Sr/86Sr=0.70836
Wing Crack, δ18O=22.5‰
87Sr/86Sr=0.70847

Figure 12

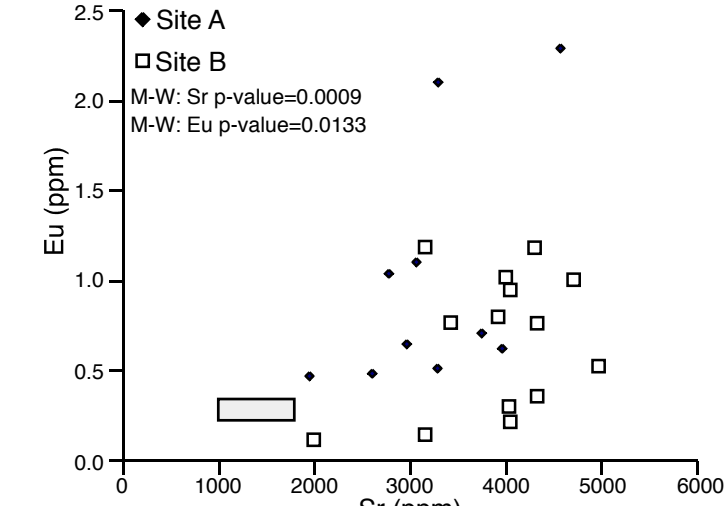
Site A
Site B
M-W: Sr p-value=0.0009
M-W: Eu p-value=0.0133
Eu (ppm)
Sr (ppm)

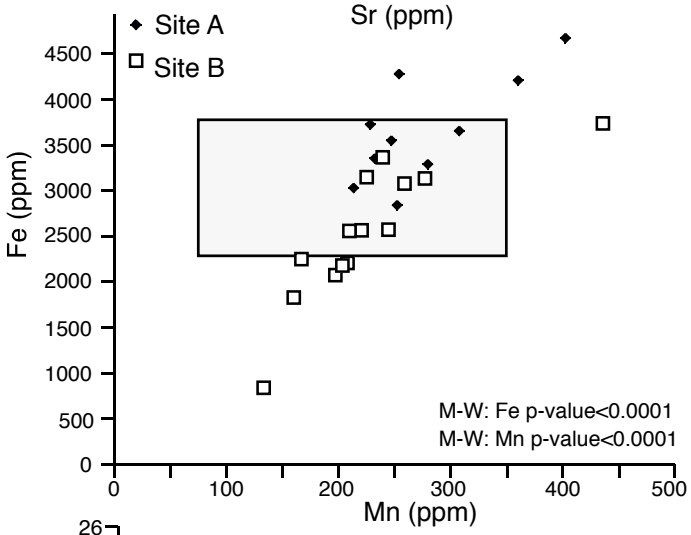
Site A
Site B
M-W: Fe p-value<0.0001
M-W: Mn p-value<0.0001
Fe (ppm)
Mn (ppm)

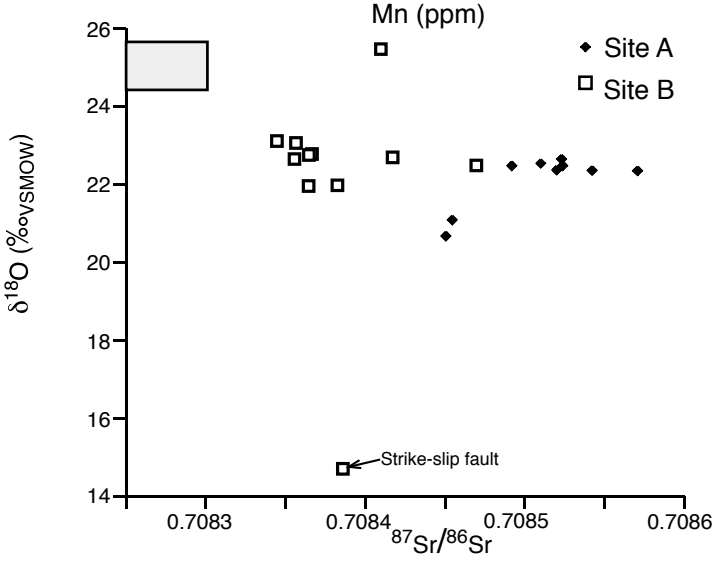
Site A
Site B
Strike-slip fault
δ18O (‰VSMOW)
87Sr/86Sr

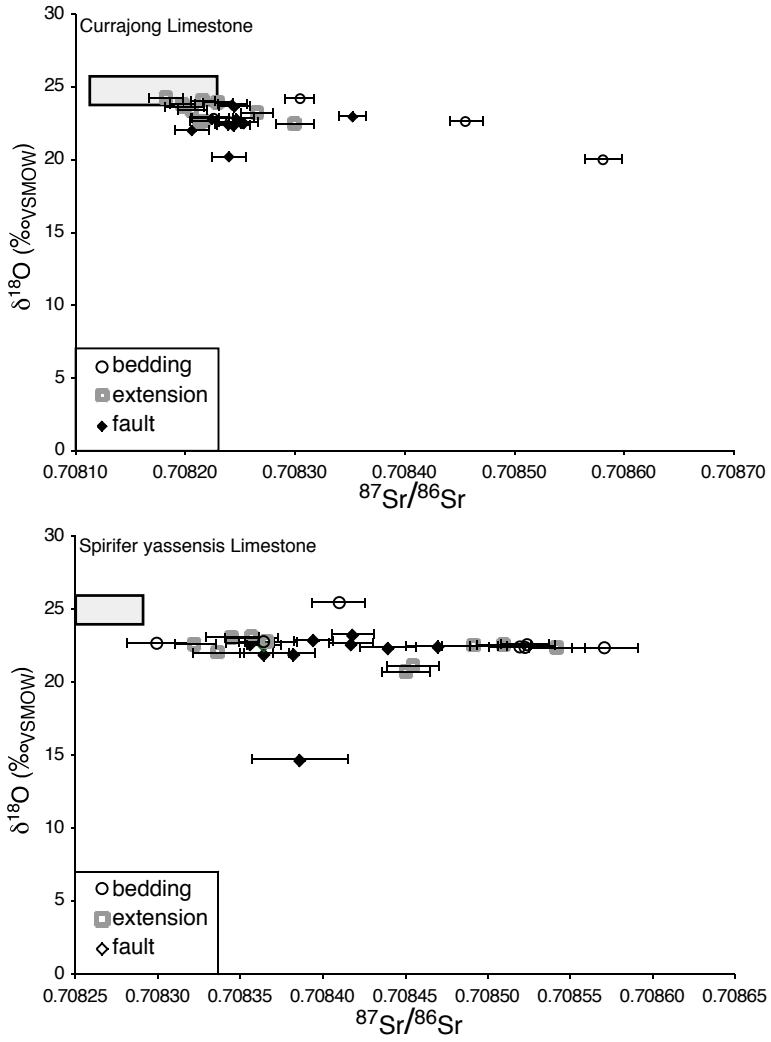
Currajong Limestone
δ18O (‰vSMOW)
87Sr/86Sr
bedding
extension
fault
Spirifer yassensis Limestone
δ18O (‰vSMOW)
87Sr/86Sr
bedding
extension
fault

Figure 14

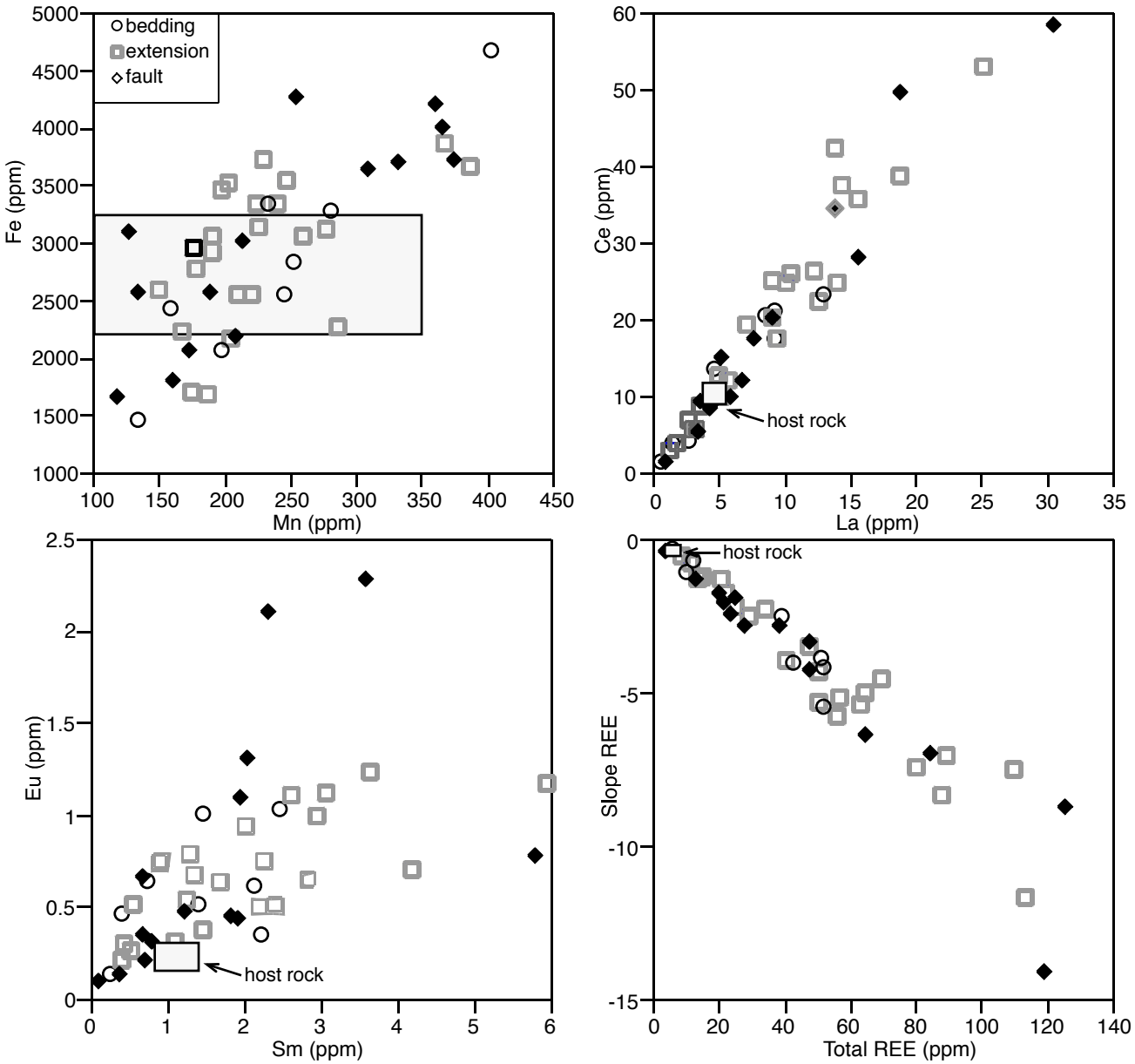
bedding
extension
fault
Fe (ppm)
Mn (ppm)
Ce (ppm)
La (ppm)
host rock
Eu (ppm)
Sm (ppm)
host rock
Slope REE
Total REE (ppm)
host rock

Figure 15

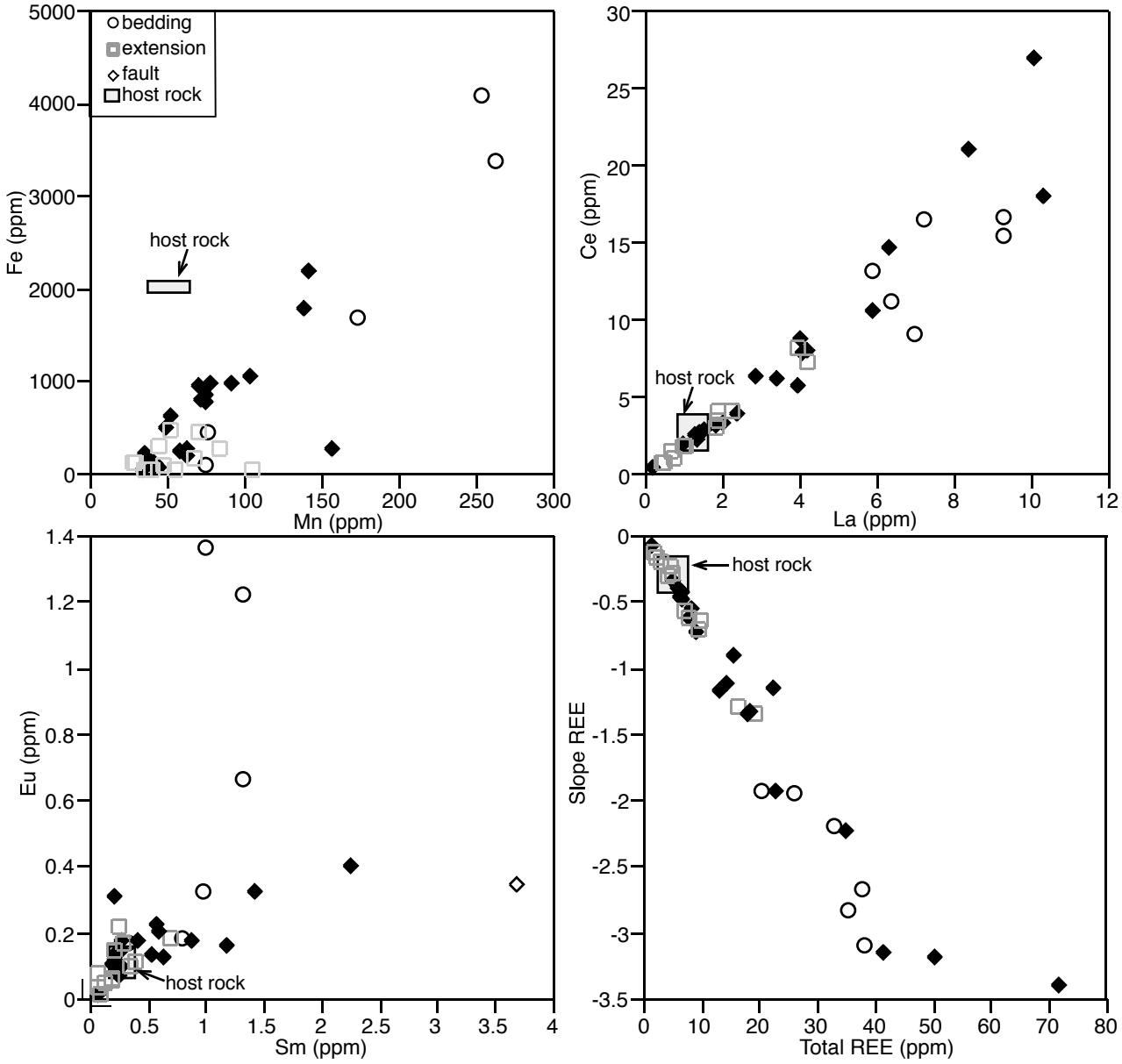
bedding
extension
fault
host rock
Fe (ppm)
Mn (ppm)
Ce (ppm)
La (ppm)
Eu (ppm)
Sm (ppm)
Slope REE
Total REE (ppm)

Figure 16